Current Opinion in Solid State and Materials Science 27 (2023) 101107

Contents lists available at ScienceDirect

Current Opinion in Solid State & Materials Science

journal homepage: www.elsevier.com/locate/cossms

High-speed nanoindentation mapping: A review of recent advances and applications

Edoardo Rossi [a,b,*], Jeffrey M. Wheeler [c,d], Marco Sebastiani [a,b]

[a] Università degli Studi Roma Tre, Department of Civil, Computer Science and Aeronautical Technologies Engineering, Via Vito Volterra 62, 00146 Rome, Italy
[b] Consorzio Interuniversitario Nazionale per la Scienza e Tecnologia dei Materiali (INSTM), Via Giuseppe Giusti 9, 50121 Florence, Italy
[c] Laboratory for Nanometallurgy, Department of Materials, ETH Zürich, 8093 Zürich, Switzerland
[d] Laboratory for Metal Physics and Technology, Department of Materials, ETH Zürich, 8093 Zürich, Switzerland

ARTICLE INFO

Keywords:
High-speed nanoindentation
Mechanical microscopy
Properties maps
Advanced materials characterization

ABSTRACT

High-Speed Nanoindentation Mapping (HSNM) has been recently developed and established as a novel enabling technology for fast and reliable assessment of small-scale mechanical properties of heterogeneous materials over large areas. **HSNM** allows for one complete indentation cycle per second, including approach, contact detection, load, unload, and movement to the n^{th} indent location, thus enabling high-resolution, spatially resolved hardness (*H*) and elastic modulus (*E*) mapping.

This article reviews the recent advancements in **HSNM** and its application to support the design, synthesis, and characterization of advanced materials, potentially impacting the ongoing digital and green transitions. A comprehensive review is given of (a) the main experimental features and critical issues of the protocols in comparison with traditional quasi-static nanoindentation, (b) the advanced data analysis tools employed, and (c) the combination with other microscopy and spectroscopy methods for multi-technique correlative applications. Finally, the relevance of HSNM for selected classes of materials is discussed, including (i) additively manufactured metals, (ii) advanced alloys, (iii) composite materials and cement, highlighting the potential for matrix-reinforcement mechanical characterization and optimization routes, (iv) coatings for industrial components and energy/transportation, discussing damage progression identification at the micro-structural level, and (v) natural materials. Ultimately, future perspectives are presented and discussed.

1. Introduction

Nanoindentation testing has emerged in the last four decades as one of the most potent tools for spatially-resolved analysis of mechanical properties at small scales [1,2].

After its original applications to surface-modified metals and coatings [3], this method has been applied to various materials and devices to investigate stiffness, strength, and fracture resistance at small scales and the related scale effects in advanced materials. This is mainly related to the reproducibility of the experimental procedures and the robustness of the Oliver-Pharr method for the analysis of hardness and elastic modulus by analyzing the nanoindentation unloading curves.

One of the first ground-breaking innovations in nanoindentation was introduced by the Continuous Stiffness Measurement (CSM) approach [2], allowing for continuous analysis of the contact stiffness (and damping coefficient) during the loading sequence. In this way, hardness, elastic modulus, and viscoelastic properties can be continuously measured as a function of the indentation depth, thus allowing for detailed analysis of the Indentation Size Effect (ISE) in metals and coatings, as well as the time and frequency-dependent properties in polymers and other strain-rate sensitive materials.

More recently, thanks to novel micro-fabrication methods, pillar testing and small-scale fracture experiments were also introduced to study the size effects in plasticity and fracture of advanced materials. Later, the possibility of installing a nanoindenter inside an SEM or TEM microscope has also opened the way to in-situ nano-mechanical testing, where deformation and failure mechanisms can be directly observed, even at high temperatures, and related to microstructural features and material's processing history.

Among many other capabilities, nanoindentation testing has emerged as an effective method for mapping the mechanical properties of heterogeneous materials. It allows for spatially resolved local

* Corresponding author at: Department of Civil, Computer Science and Aeronautical Technologies Engineering, Via Vito Volterra 62, 00146 Rome, Italy.
E-mail address: edoardo.rossi@uniroma3.it (E. Rossi).

https://doi.org/10.1016/j.cossms.2023.101107
Received 3 July 2023; Received in revised form 20 September 2023; Accepted 21 September 2023
Available online 3 October 2023

hardness and elastic modulus analysis, with a resolution that depends on indentation depth and spacing. This method, also known as statistical or "grid" nanoindentation [4–6], was introduced in the early 2000s for applications in biomaterials and cement-based composites. Some examples of early applications of grid nanoindentation are shown in Fig. 1, where the relevance of this method for mechanical phase analysis in multiphase materials and composites is highlighted.

In particular, the early works of Ulm and co-workers [6–10] contributed to defining the main principles of this technique, consisting of three main steps: (a) realization of a matrix of nanoindentations (with given maximum depth, or load, and spacing), (b) statistical deconvolution of elastic modulus and hardness data to identify mechanical phases of the material and (c) correlation with microstructure by comparison with microstructural observations (optical, SEM, EDS, EBSD, etc.) of the same area. The experimental workflow starts with the proper choice of the maximum indentation depth $\boldsymbol{h}$ and spacing $\boldsymbol{d}$, which should be selected based on the average dimension of grains and/or phases and the surface roughness of the sample. The selection criteria are, usually, that (a) spacing $\boldsymbol{d}$ should be, at the same time, lower than the average grain size and five times higher [11] than RMS roughness (where the roughness is measured over a scanning size 200 times $\boldsymbol{h}$). A recent study has also demonstrated that minimum indent spacing should be ten times the indentation depth for a Berkovich tip to reduce mutual interactions between indents [12].

One of the first applications of this technique was to cement-based composites, which show the presence of multi-scale microstructural features ranging from nanometers (colloidal nanometric units) to tens of micrometers (large capillary pores). Most of the literature agrees on the existence of at least two different calcium silicate hydrate (shortly C–S–H) phases in Portland cement pastes, namely high-density (HD) and low-density (LD) C–S–H, differing for the packing density of the nanometric elementary building blocks. The complexity of these materials is further increased due to the extensive use of additives [13], and high-resolution nanomechanical mapping tools are becoming increasingly important.

The case of battery composites [14–16] is relevant to highlight the main strengths and weaknesses of conventional nanoindentation mapping. In a recent work, a $LiMn_2O_4$ composite cathode was analyzed and discussed. In this case, the sample exhibits great differences between the matrix and the particles in terms of both hardness and modulus, combined with a high level of porosity and micro-cracks, which in turn resulted in a significant scattering of the data because of the numerous experimental artifacts (edge effects, structural compliance of the particles, porosities, interfacial delamination, etc.). The proposed solution was a two-step filtering method of the data, through which only valid tests were selected for statistical deconvolution [15]. The two filtering parameters aim at considering only the (a) quadratic load versus displacement curves and (b) the curves showing a constant $\boldsymbol{S^2/L}$ signal as a function of depth (where $\boldsymbol{S}$ is the contact stiffness as measured during CSM nanoindentation and $\boldsymbol{L}$ is the applied load).

On the one hand, the proposed filtering method resulted in a remarkable improvement in the signal-to-noise ratio and better accuracy in determining the mechanical properties of the $LiMn_2O_4$ particles. On the other hand, applying such a filter also significantly reduced the number of valid tests for statistical deconvolution, where more than 80% of tests are cut-out by the filtering method on the analyzed $LiMn_2O_4$ composite. This result clearly showed that the increase in the number of measurements (from hundreds to thousands) represents a critical (game-changing) factor for the possible validation of the method and the establishment of standard operating protocols in real industrial samples.

These two examples on cement and battery composites demonstrate that the use of quasi-static nanoindentation is not adequate to reach the required test numerosity for reliable application in industrially relevant complex cases (e.g., advanced nano-composites, complex multiphase steels, composite biomaterials, etc.).

In recent years, and in particular, starting from an early publication of J. L. Hay in 2013 [17], instrument manufacturers have proposed novel developments in both nanoindentation hardware and software to

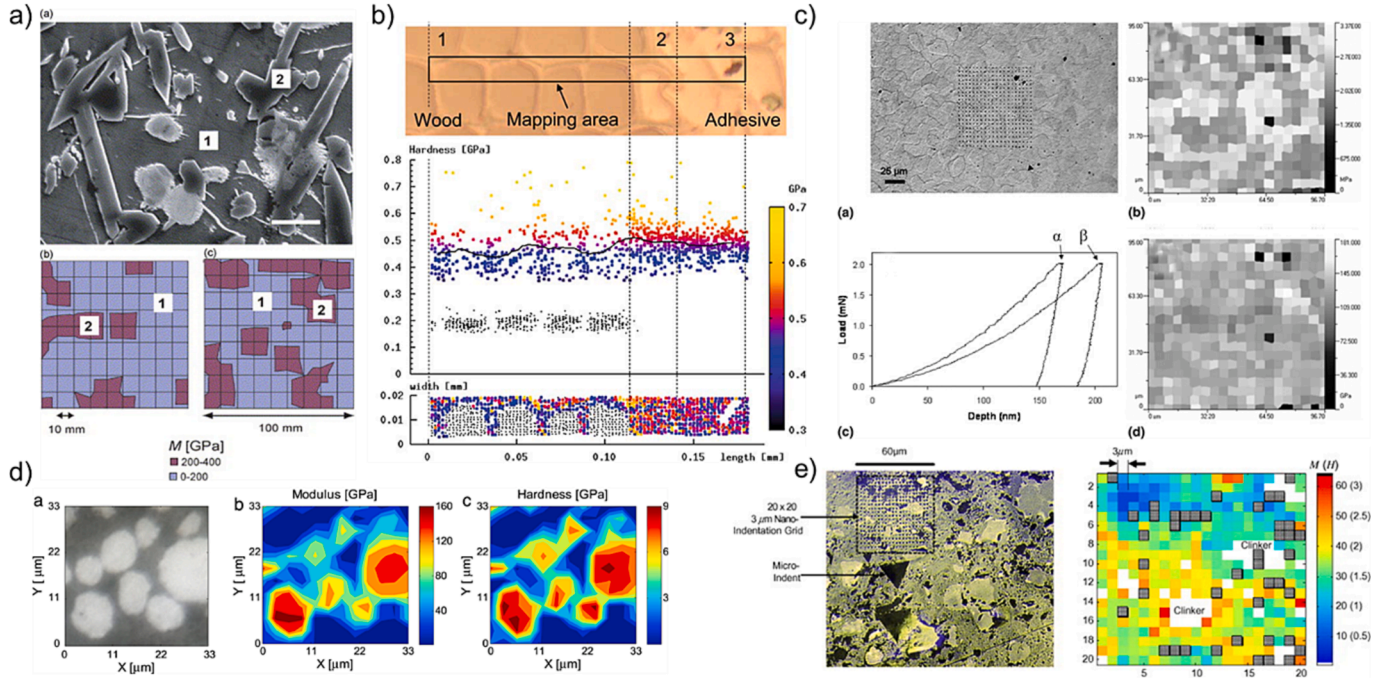

Fig. 1. Early application examples of grid nanoindentation testing: a) multi-phase 70Ti-30TiB phase identification via mechanical mapping of indentation moduli (M) (reprinted from Constantinides, G. et al. [7], Copyright(2006), with permission from Elsevier); b) wood-adhesive bond interface region (reprinted and adapted from Konnerth, J. et al. [19], Copyright(2007), with permission from Springer Nature); c) polished α-β brass (reprinted from Randall, N. X. et al. [9], Copyright (2009), with permission from Springer Nature); d) composite LiNi0.5Mn0.3Co0.2O2 cathode (reprinted from Vasconcelos, L. S. de et al. [20], Copyright(2016), with permission from Elsevier) and e) cementitious materials w/c = 0.3 paste (reprinted and adapted from Ulm, F. J. et al. [21], Copyright(2010), with permission from Elsevier).

increase the speed of nanoindentation mapping, in comparison with conventional testing, without losing accuracy and resolution. This work applied the new "high-speed" method to a magnesium alloy, showing that high-throughput mapping can be a powerful tool to identify mechanical phases in multi-phase metals. The primary factor that differentiates high-speed nanoindentation from conventional nanoindentation is simply the reduced time to complete an entire indentation cycle (i.e., surface approach, contact, load, unload, retraction, and stage movement to a new test location), which typically around or less than 1 s (one second).

After development, this new high-speed method was applied to battery composites [16] and cementitious materials [13]. In the latter case, high-speed nanoindentation was combined with SEM/EDS mapping to investigate the microstructural evolution of hydrated phases in cement pastes, as a function of the hydration time (from 1 to 28 days), for the first time. In this article, the conventional nanoindentation mapping is directly compared with the novel high-speed method, showing that some phases could not be identified by a conventional nanoindentation map (of 400 measurements). On the contrary, the high-speed maps (made of roughly 40,000 tests) allowed for high-resolution microstructural mapping of all existing phases (including UHD, HD, and LD C-S-H, the tri- and di-calcium silicates (C2S and C3S), the calcium aluminate and ferrite (C3A and/or C4AF). In addition, results showed that the intrinsic elastic moduli of the hydrated C-S-H phases are independent of hydration time, thus confirming that they are uniquely related to discrete packing density levels. This demonstrated two advantages of high-speed nanoindentation: simultaneous numerosity and high-speed for time-resolved experiments.

Moreover, a work employing high-speed nanoindentation to investigate mechanical properties variations as a function of the interdiffusion of alloys-forming elements has been carried out by Wheeler et al. [18], which first demonstrated how thermodynamical equilibrium diagrams could be fully reconstructed in terms of their constitutive phases via combined EDS and HSNM.

The purpose of the present review article is to delineate how this method has evolved in recent years, thanks to further developments in (a) the nanoindentation testing protocols, (b) the data analysis tools, and (c) the combination with other microscopy and spectroscopy methods. In turn, we will show how the recent developments open the way for applying this method to complex and industrially-relevant materials and devices, potentially impacting the next digital and green transition challenges. The article is structured as follows: first, we will review the critical experimental issues when making large areas of high-speed nanoindentation maps and the data analysis and interpretation tools. Then, the potential of correlative mechanical microscopy (i.e., the combination of HSNM with microscopy and spectroscopy tools) is discussed. Finally, a comprehensive review of applications for critical materials and innovation markets is given, leading to conclusions and perspectives.

2. Critical experimental issues in high-speed nanoindentation mapping

Before understanding the benefits of high-speed nanoindentation, reviewing and analyzing the main shortcomings and differences concerning quasi-static and CSM nanoindentation testing is essential.

High-speed testing usually provides different information than CSM nanoindentation, where contact stiffness is continuously acquired during the experiment. In the most common fast testing configuration, only a single stiffness data point is acquired in correspondence with the maximum load, thus allowing for a single *(E, H)* data point for each *(x;y)* position. With this in mind, selecting the maximum indentation depth (and indentation spacing) is paramount, especially in those cases (thin films, multi-phase materials) where a depth dependence on mechanical properties could be expected. However, some systems do allow high-speed mapping to be performed with CSM nanoindentation (sometimes referred to as 4D mapping), where a discrete series of stiffness data can be acquired as a function of depth, thus allowing for the calculation of hardness and modulus at discrete depth data points. This requires high oscillation frequencies to collect these data points at high displacement rates during testing and an absence of system resonance frequencies below the acquisition frequency, which is challenging.

Another typical feature of high-speed nanoindentation to be kept in mind when designing experiments is the relatively high strain rate resulting from the high speed of the test. This must be carefully evaluated for those materials that show a pronounced strain rate sensitivity (e.g., thermoplastic polymers and superplastic metals), where the calculated hardness values could deviate remarkably from those evaluated by quasi-static testing.

High-speed nanoindentation mapping provides several unique technical challenges. Many of these are hardware-related, especially regarding the sampling rates, system resonance frequencies, positioning speed and accuracy, and actuation speeds. This extends to environmental and system stability for *operando* mapping in different humidity, temperature, or other environments. These are challenges for system manufacturers, who have recently enabled many of these technologies.

From the researcher's perspective, achieving maps with the highest resolution and sensitivity over a vast area is desirable. Consistency in the sampled volume (Representative Volume Element, RVE) for each data point is essential for a mapping technique to achieve its optimal resolution. This means that the size/depth of the indentations and their spacing should be consistent, as well as the tip area function during the entire test duration. This raises the question of how closely the indentations can be spaced and how small they can be made while still yielding representative values. Additionally, the tip should remain effectively sharp without significantly changing its diamond area function in cases where defects, cracks, and porosities are present. In this section, we will discuss these issues.

2.1. Indentation spacing criteria

Assuming that the size of the indentations is consistent and the material is homogeneous, how closely spaced can the indents be placed? Traditionally, the criterion of Samuels and Mulhearn [22] requires that indentations should be spaced no closer than three times the width of the indentation, which is 20× the normalized spacing vs. indentation depth (d/h) for a Berkovich indenter. This is based on the concept that the plastic zones of neighboring indentations should not touch. This is the criterion used in several ASTM and ISO standards.

Indentations can be spaced as closely as desired for elastic contacts for elastic modulus mapping, neglecting hardness. However, the resolution of this technique will depend on the probe radius.

Phani and Oliver [12] investigated this criterion in 2019 through extensive 3D finite element modeling and experimental validation. They determined that a significantly closer spacing (10 d/h or 1.5× the width of the indent) was achievable without significant interference for most homogeneous materials - Fig. 2a. This was rationalized by the fact that the outer portions of the plastic zones could be allowed to touch without a significant strain-hardening effect on the majority response of the indentation - Fig. 2b.

Further, they investigated the influence of different indenter angles and determined that the recommended indentation spacing remains constant at 1.5× the width of the indent, regardless of the indenter angle. Higher aspect ratio/cone angle indenters, e.g., a Cube Corner, penetrate deeper to achieve a given indentation width, but the indentation spacing remains constant. Therefore, higher aspect ratio indenters may allow higher depth indentations to be performed for a given indentation size, producing a stronger hardness signal, but this would be at the cost of the stiffness/modulus response.

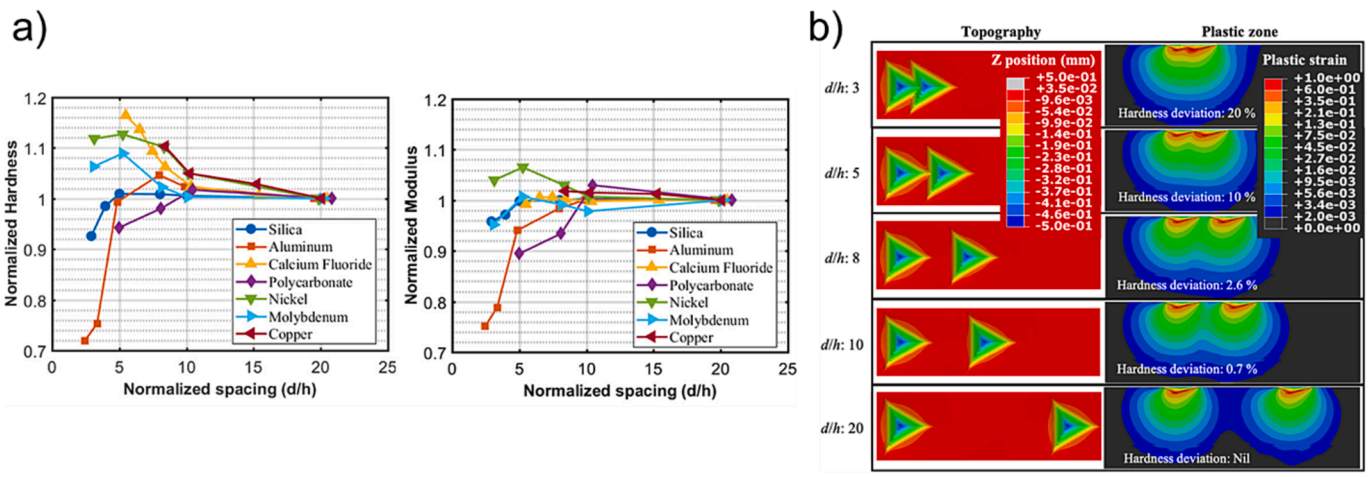

Fig. 2. Influence of inter-indentation spacing on HSNM measurements for different materials a) evidencing errors in hardness and modulus measurements as a function of normalized spacing, based on b) FEA calculations of the plastic zone and deviations in hardness on plastic work criterion. Reproduced from Phani et al. [12].

2.2. Load or displacement targeted mapping

In high-speed mapping via nanoindentation, the load and depth targets are critical objective functions regulated dynamically through the instrument's control system feedback loops. While pure load-controlled nanoindenters can rapidly attain load targets through direct force control, they depend on a reactive process to meet depth targets, continually adjusting displacement based on the force applied. Conversely, displacement-controlled nanoindenters can quickly reach depth targets but require an adaptive retroaction mechanism to meet load targets, ensuring meticulous evaluations across regions with varying hardness.

To ensure that all indentations meet the given spacing criterion in a heterogeneous or multi-phase material, which is usually the case for materials of interest for mapping, it is essential that the largest indentations or the indentations in the softest region/phase still meet this criterion. If a map is performed with a maximum displacement target, indentations are all performed to the same maximum depth (upper grid in Fig. 3a). This ensures similar indentation sizes with only minor variations from differences in elastic recovery. In this case, a given spacing/depth for a map can be directly specified.

When mapping using a maximum load target, the applied load must be carefully selected. One way of rapidly determining the appropriate load for a desired mapping resolution/spacing is by performing a widely spaced grid with a gradient in load so that the load is progressively decreased for each indentation in the grid. This produces a plot like that shown in Fig. 3b, where the load-depth relationships can be quickly visualized for the two different phases in the indented area. From this type of plot, the lowest load to achieve a given depth can be quickly selected, e.g., ~0.75 mN for 150 nm depth/spacing. However, this still results in a grid where the indentation's size depends on the materials' hardness - Fig. 3a. This is useful for visual interpretation of the indentation grids during microscopy, as the harder phases are directly apparent through their smaller indentation sizes.

To understand the effects of using load or displacement targets on mapping results, it is instructive to examine the variation that emerges from applying such targets when mapping a microstructure containing highly mechanically dissimilar phases - Fig. 4. These results (adapted

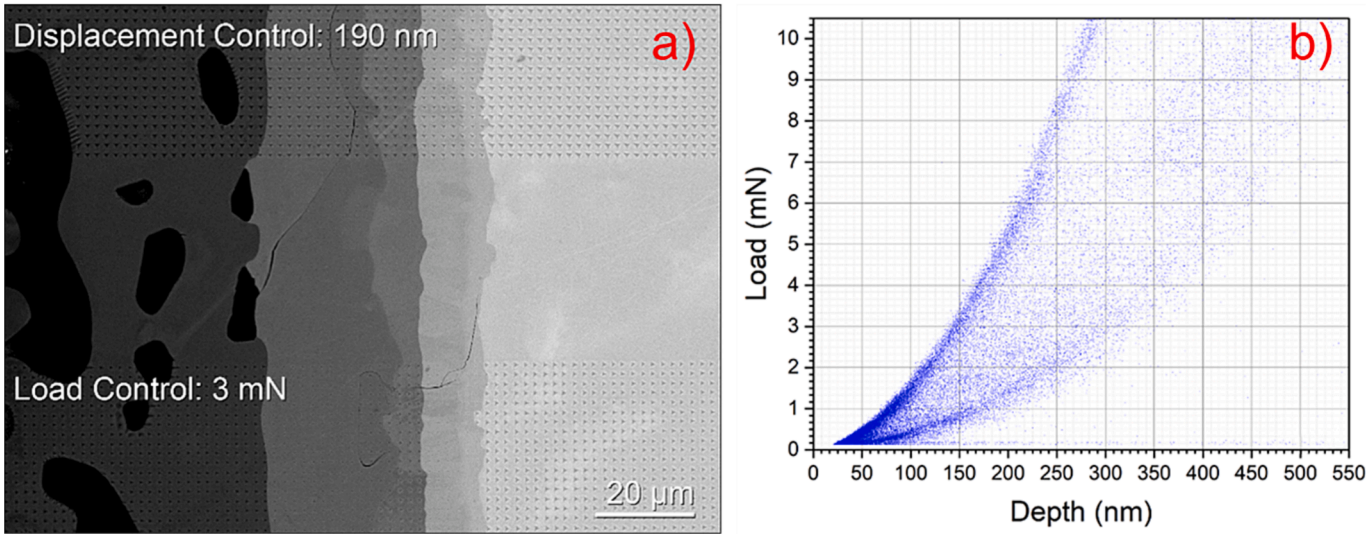

Fig. 3. Influence of load vs. displacement targets in indentation size in mapping: (a) Grids of indentations made across a Ni-Ta diffusion junction with both load and displacement targets, illustrating the relative influence of local hardness on indent size in both modes (reprinted and adapted from Wheeler, J. M. et al. [18]), (b) load-depth relationships in a two-phase Al-Cu eutectic alloy shown by a grid of indentations with progressively decreasing load (reprinted and adapted from Besharatloo, H. et al. [23]).

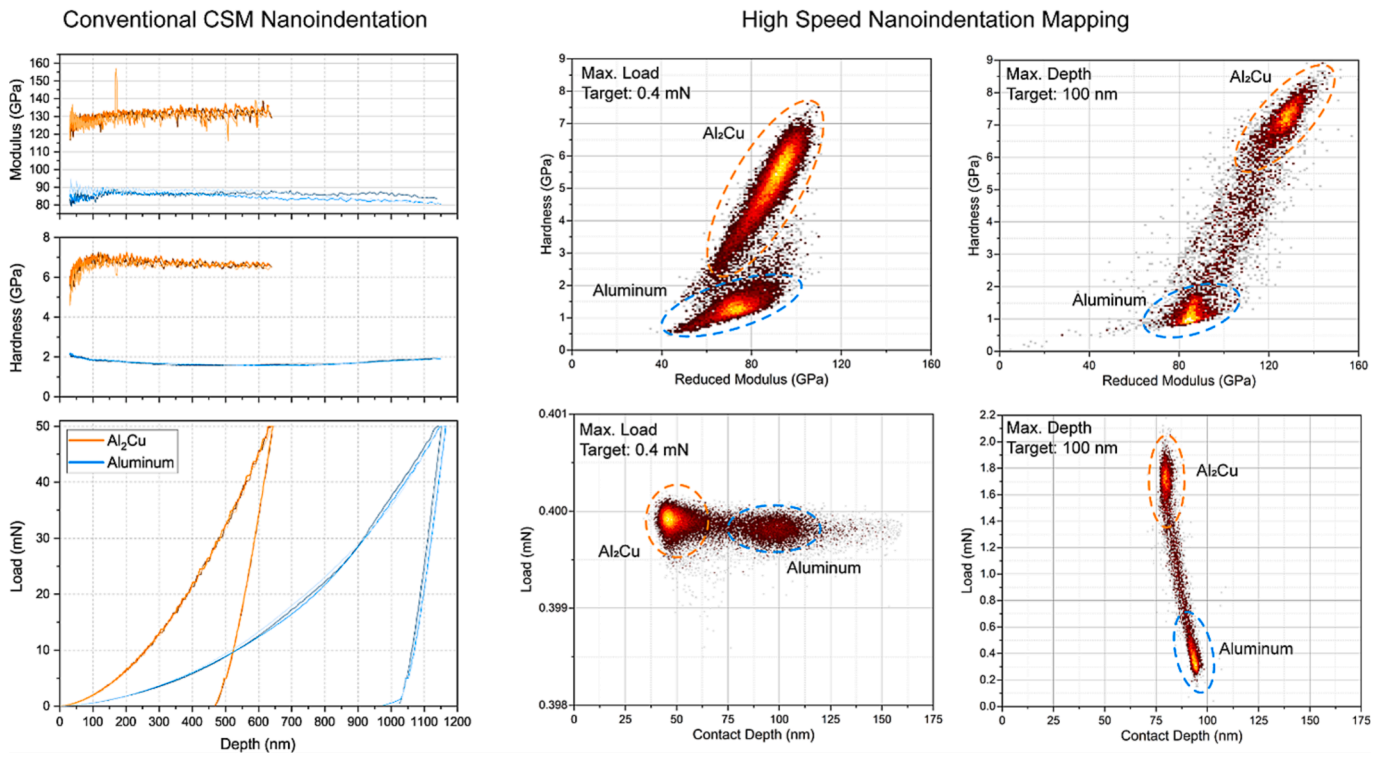

Fig. 4. Comparison of indentation results (reprinted and adapted from Besharatloo, H. et al. [23]) acquired by conventional CSM nanoindentation and high speed nanoindentation mapping using either maximum load or maximum depth targets on an Al-Cu eutectic sample.

from [23]) were acquired from the same Al-Cu eutectic sample, containing a fine microstructure of aluminum and Al_2Cu phases. Both load and depth targets were selected for producing indentation maps with a spacing of 1 μm and a maximum indentation depth of around 100 nm. A maximum load target provides a precisely determined maximum load in both phases. However, due to the difference in hardness between the two phases, the scatter in contact depths in the two phases is >2×, which implies a proportionally larger variation in contact areas and contact stiffnesses. The max. load target was selected to ensure that all indentations have a contact depth of less than 100 nm to satisfy the 10 *d/h* criterion for the 1 μm spacing. However, this was partly unsuccessful, suggesting some indentations in the softer Al phase likely interacted. Using a maximum depth target of 100 nm, all indentations are seen to have contact depths (after elastic unloading) of less than 100 nm, with the contact depth decreasing with the hardness/modulus ratio of the phases due to elastic recovery.

Attained load values for the max. depth target shows a vast spread, with the harder Al_2Cu phase producing loads over 4× greater than the max. load criterion. Neither max. load nor max. depth criteria produce indentations of perfectly matching contact depths due to elastic recovery during unloading, but the size variation is significantly reduced using a max. depth target. For a system with consistent measurement sensitivity using either target criterion, it is clear that a max. target depth criterion would provide much greater and more consistent contact stiffness measurements from a microstructure with dissimilar phases. This is due to greater contact depths, loads, and contact stiffnesses achieved in the harder phases while still satisfying the spacing criterion to prevent overlapping indentations in the softer phase. Hardness and elastic modulus value distributions resulting from the two criteria suggest this. Significantly more precise property distributions are noticeable in the max depth criterion. Further, using a max. depth criterion, the property distributions are more accurately located at values consistent with conventional CSM indentation values measured at depths of 100 nm.

As introduced at the beginning of this section, it is important to note that both settings (maximum depth or load targets) can be set in displacement- or force-controlled nanoindentation systems. The achievable speed of HSNM with each system then depends on whether it is operated in its native mode and its control feedback loop speed.

The influence of contamination on mapping with load or displacement targets is also worthy of note. HSNM with a load target is less prone to measurement errors from the presence of soft debris over the tested surface. Mapping with a maximum load target depends less on detecting the initial contact displacement, so surface contamination is primarily ignored during mapping. During operation with a displacement target, an initial contact detection threshold must be set in terms of measured load/stiffness/et cetera to determine the contact displacement, such that a target maximum displacement can be precisely achieved. This contact threshold can be set to a higher level to increase tolerance to contamination, but this decreases the precision to which the depth target can be achieved in either load or displacement-targeted operation. Contamination may accumulate on the indenter during mapping, typically at a depth similar to the median max. depth. This contamination can increase the local contact area between the indenter and sample and the apparent contact stiffness. Thus, it is important to maintain indenter and sample cleanliness, particularly for indentation mapping at lower penetration depths.

Since both force and displacement control methods can produce variation in contact depth, indentation size effects can still influence the consistency of measurements taken using either criterion. However, that influence would be expected to be greater when using a max. load target. The magnitude of indentation size effects varies among various materials significantly with well-annealed, soft metallic single crystals showing relatively large size effects and work-hardened, hard, or nanocrystalline materials showing relatively small effects [24]. To ensure that an absolute comparison could be made between the properties of dissimilar phases at a selected indentation size, indentation mapping would ideally be performed using a constant indentation strain rate using a continuous stiffness measurement technique (e.g. NanoBlitz 4D), so that data can be selected from matching depths for comparison under the same experimental conditions.

For indentation mapping at very shallow depths ($h \ll 50$ nm), careful surface preparation is extremely important to ensure adequately low surface roughness and remove any subsurface damage from materialographic preparations. At such low depths, significant influences have been seen in indentation measurements due to "pop-ins" attributed to cracking of surface oxide layers and intermittent plastic flow due to dislocation nucleation/avalanches [25]. Such events will likely increase the scatter or noise in indentation mapping results, as hardness could appear quite high before a pop-in or crack but very low afterward. A similar scatter in modulus measurements would likely be observed, as well.

2.3. Lateral resolution limits

With the depth/spacing ratio established for a consistent indentation size, the question remains: How small can indentations be made, while keeping reliable quantification of hardness and modulus? In other words, what is the maximum lateral resolution of this technique? This depends on both the indentation system's sensing resolution and the sharpness of the indenter probe. If we assume the first is sufficient, then how small can indentations be made? This was explored by Hintsala et al. [26] using a range of Berkovich indenters of different sharpness or tip radius on fused silica – Fig. 5. This article quantified the minimum indentation depth ensuring the full transition from elastic to elastic–plastic deformation.

They concluded that reliable hardness values could be obtained at depths of at least 15 nm on fused silica, as the Hertzian pressure underneath the tip was sufficient to cause stable yielding. If we apply the spacing criterion of 10 d/h from Section 2.1, then this suggests lateral mapping resolutions of 150 nm are achievable with a sufficiently sharp indenter. This indicates that the strength of the material also limits the ultimate resolution of the technique. If the material's elastic yield point is higher, a higher depth would be required to cause yielding. Conversely, a softer material may allow higher-resolution mapping. As fused silica is a relatively hard material, achieving even higher-resolution maps in many materials may be possible.

At such small fine resolutions, the accuracy of the sample positioning stages is also an important consideration - Fig. 6. To ensure 95% (2σ) of indentations meet the 10× criterion, the spacing should be: $L = 10d + 4\sigma$, where σ is the standard deviation of the positioning accuracy or noise floor. The extra 4σ is required to ensure that positioning error does not result in two neighboring indentations failing to achieve the desired

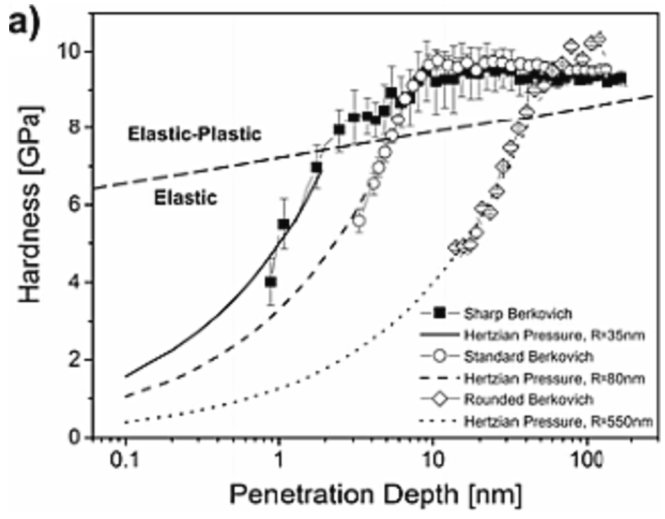

Fig. 5. Measured hardness vs. penetration depth for Berkovich indentations into fused silica for tips of varying sharpness.
Reprinted from Hintsala et al. [26].

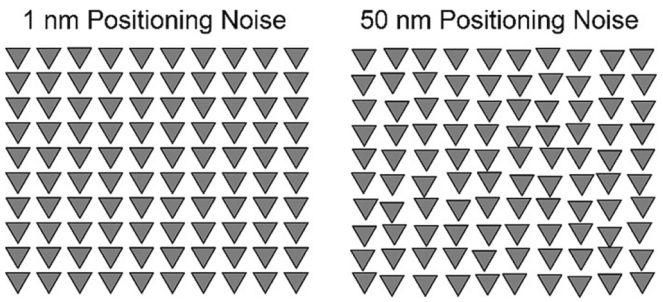

Fig. 6. Schematic illustration of the influence of positioning noise on the regularity of an indentation grid with a 1 μm inter-indent spacing – high noise relative to the indentation spacing risks interactions between indentations and limits the feasible resolution.

spacing criterion. This relationship scales with spacing, so indentation grids with smaller inter-indent spacings require higher precision positioning.

The lateral resolution limits imposed by the minimum achievable indentation size for hardness measurement, plastic zone radius, and positioning noise also pose a relevant question on interpreting high-speed mapping data plots. A significant issue raised in the previous sections is the disparity between the interaction volumes for the probed elastic and plastic responses. The plastic zone has a gradient in strain and varies in size/shape with local microstructure. The elastic zone similarly varies with microstructure but is much larger and, in principle, does not have any clear boundary due to the intrinsic nature of elasticity itself. As the indenter resolution has three contributions and consists of differently-sized elastic and plastic zones [26], plotting must also be consistent and will have intrinsically different sampled volumes between the reported elastic modulus and hardness maps. Particular care must also be taken in contour plotting, which presents an interpolated version of the data, being the measured properties interpolated linearly between each point.

2.4. Influence of indenter tip condition

As discussed in Section 2.2, the indenter's tip radius significantly influences the maximum resolution attainable using indentation mapping. This raises the question: Does the tip wear out during the thousands of indentations performed for a map? An indenter needs to be sufficiently sharp to generate a representative hardness value for its nominal cone angle, or the results will not be able to be replicated by other laboratories. This also implies that the shape of the indenter must be consistent during the mapping procedure, or the results will shift during the map: a phase might gradually or suddenly appear harder as the indenter is scanned, whereas previously, the values had been consistent. This can result from surface roughness or pores, surface contamination, or indenter wear.

If the measured values shift during mapping, it can be helpful to examine both the hardness and elastic modulus results to determine the cause. If both H and E values suddenly shift and then return to previous values, then surface roughness or porosity is the likely cause. If the E values suddenly increase and leave a streak across the map, but the H only slightly increases, then it is likely that surface contamination has adhered to the tip, changing the effective tip shape. Contamination removal requires tip cleaning, such as high load indentations into Bakelite. If H and E values decrease, then it is likely that some contamination has been gradually pushed up the indenter or there is an error in the analysis, as indenter geometries tend not to sharpen with wear. If both the H and E gradually increase during many indentations or a high-temperature map, then the indenter may be experiencing wear.

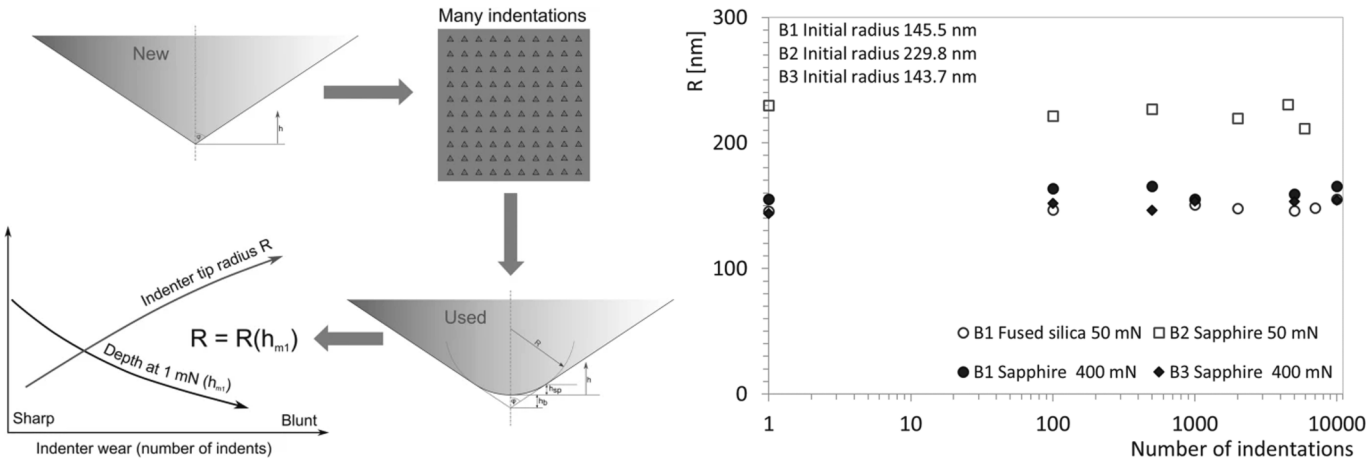

Fig. 7. Estimating the indenter tip radius R after increasing the number of indentations at 50 mN or 400 mN on fused silica and sapphire. (reprinted and adapted with permission from [27], Copyright(2021), with permission from Springer Nature).

2.4.1. Mechanical wear

The likelihood and magnitude of mechanical tip wear were systematically investigated by Nohava et al. [27]. They performed indenter wear tests by performing up to 10,000 indentations at loads of 50 mN and 400 mN on fused silica and sapphire - Fig. 7. They monitored the effective indenter radius by several parameters measured during the indentation, such as penetration depth, H, and E values. The results showed only minor changes during most tests, with the values remaining consistent within the measurement precision, and even 10,000 indentations at 400 mN on sapphire resulted in only a ~7% increase in the tip radius. Given the relatively high hardness of sapphire, this indicates that mechanical wear does not have a large effect on a 100 × 100 indentation map, save perhaps on superhard materials [28].

2.4.2. Chemi-mechanical or high-temperature wear

Tip wear mechanisms change at high temperatures. At elevated temperatures, the chemical potential between the indenter tip and sample becomes increasingly influential [29,30]. This enables pure, soft iron to rapidly react with diamond indenters at high temperatures to form iron carbides – significantly blunting a tip and changing its geometry. An example of this is shown in Fig. 8, where atomic force microscopy was used to investigate the tip radius of a probe before and after high-temperature indentation [31]. Indeed, even atmospheric oxygen will damage the indenter if a high vacuum nanoindentation system is not employed. Oxidation is also a concern for maintaining a high-quality sample surface for mapping. Indenter-sample reactions are a significant challenge for high-temperature indentation mapping and a limiting factor for high-temperature mapping resolution. Indentations must be made sufficiently deep and widely spaced for any indenter wear to be negligible.

The consensus is that diamond indenters are preferred for light metals (excluding titanium), coinage metals, or hard materials such as ceramics at high temperatures [30]. However, carbide-forming or carbon-absorbing materials like ferrous and refractory metals require an alternative to diamonds. The current recommendation is monocrystalline tungsten carbide indenters, but this is under active investigation [32].

2.5. Effects of strain rate in high-speed nanoindentation

The indentation strain rate $\dot{\varepsilon}$, displacement rate $\dot{h}$, and loading rate $\dot{P}$, are related through the following equation [33,34]:$\dot{\varepsilon} = \frac{\dot{h}}{h} \approx \frac{\dot{P}}{2P}$. By controlling the displacement or loading rate to achieve a constant strain rate, nanoindentation results may be acquired at a desired strain rate. This provides much more consistent values than constant displacement or loading rates, which produce gradients in strain rate versus depth. Due to system control loop speeds, constant strain rate indentation is usually limited to strain rates $\leq 0.1 s^{-1}$. High-speed nanoindentation involves higher loading/displacement rates. However, for most current systems, the approximate indentation strain rate during high-speed nanoindentation mapping is $\dot{\varepsilon} \approx$ 5–10 s^{-1} [35]. This is still several orders of magnitude below the high strain rate regime, $\dot{\varepsilon} > 10^3\ s^{-1}$, where strain rate sensitivity sharply increases, but this rate increase may be significant for many materials.

The influence of strain rate variations on measured indentation values can be estimated by considering the materials' strain rate sensitivity (SRS) using the equation: $m = \partial(lnH)/\partial(ln\varepsilon)$, where m is the strain rate sensitivity, H is the hardness, and ε is the strain rate. As high-speed indentation is typically estimated as being ~100× faster than conventional indentation, one can estimate a similar two-order-of-magnitude increase in strain rates. Since typical m values range from 0.001 to 0.1 in crystalline materials, this would result in a hardness variation between 0.4% and 37% compared to conventional nanoindentation [26]. This is a significant consideration, especially for materials with higher strain rate sensitivity values and locally varying strain rate sensitivity in multi-phase samples. Therefore, we can conclude that particular care should be given to those materials showing a pronounced strain rate sensitivity. The data from high-speed indentation could differ significantly from those obtained by quasi-static measurements. To address this, it is suggested that high-speed maps may be performed with constant indentation strain rates or indentation strain rate jumps [36] to characterize this phenomenon. While the strain rates achievable using such methods are currently limited; it is expected that advances in hardware will enable these soon.

2.6. Methodological comparison: High-speed nanoindentation mapping vs. ISO 14577 and CSM grid indentations

With the groundwork established in the previous sections through the dissertation of the high-speed mapping distinctive features and experimental issues, we now pivot to systematically comparing high-speed nanoindentation mapping, Continuous Stiffness Measurement (CSM), and ISO 14577 [37] nanoindentation. This section aims to discuss their respective attributes and limitations through the comparative analysis of measurement results and data analysis approaches (inextricably linked to the performance of high-speed mapping) on

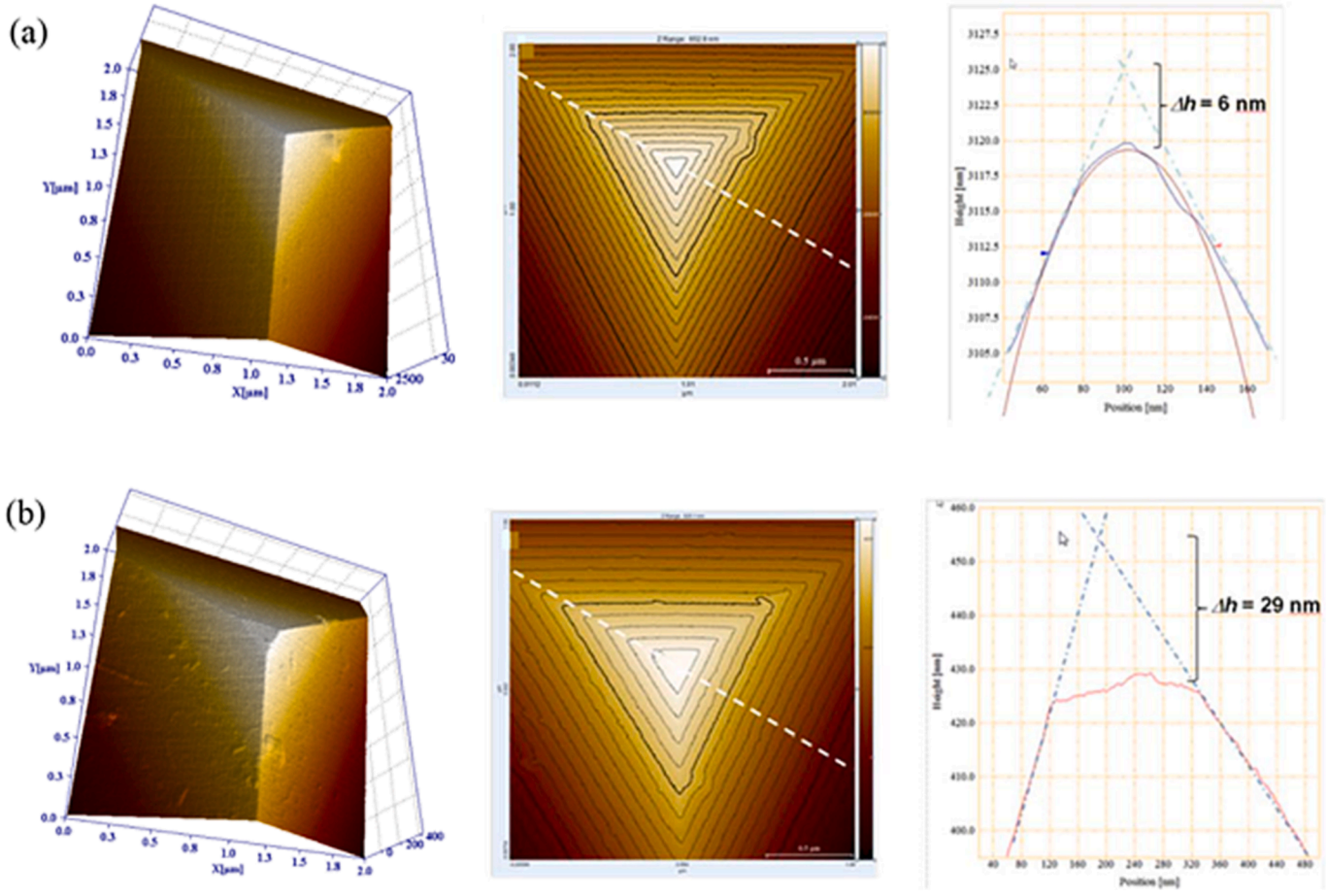

Fig. 8. High-temperature indenter tip wear revealed by AFM of a new indenter (a) and the same indenter after use at 200 °C on amorphous SiC (b). Reprinted and adapted from Monclús et al. [31], Copyright(2014), with permission from Springer Nature.

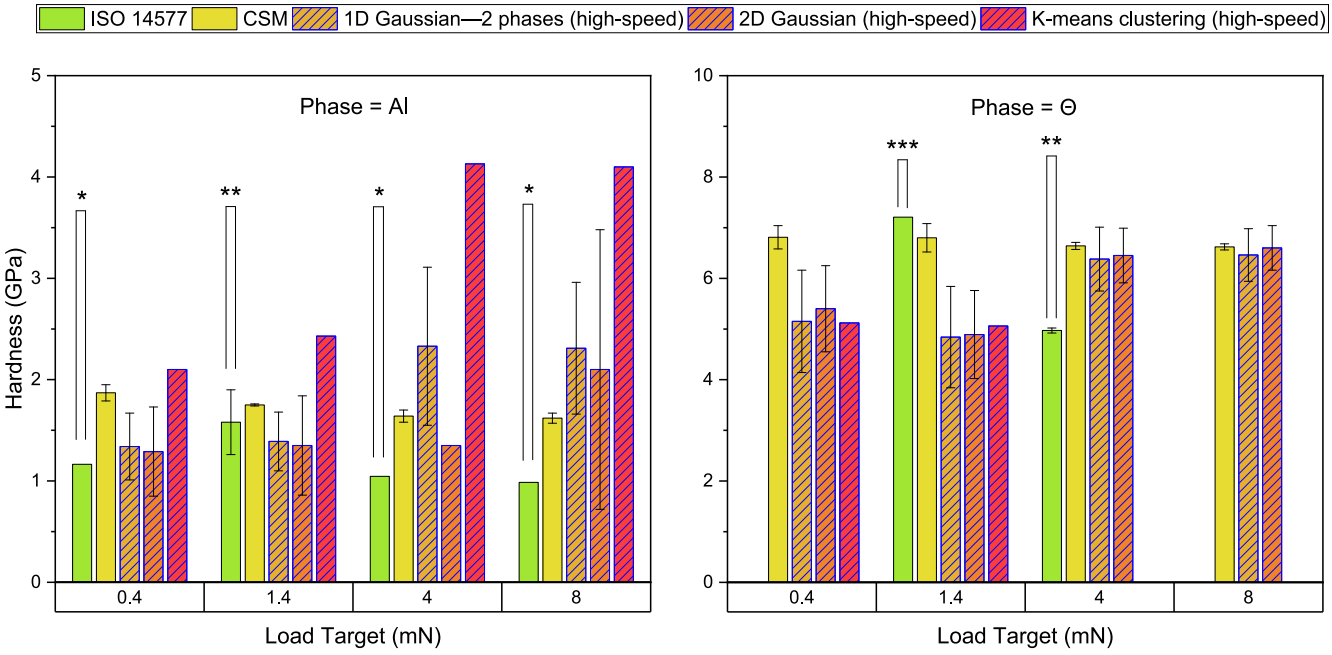

Fig. 9. Bar chart depicting differences in hardness measurements across nanoindentation methodologies, loading conditions, and material phases for an Al-Cu eutectic sample (high-speed data is taken from Besharatloo et al. [23]). Other literature data (i.e. refs from [38–40]) is represented, respectively, with *, **, *** symbols for readability).

representative material systems. We attempt to deconvolute the interplay of spatial resolution, dynamic response, and standardization by dissecting their technical underpinnings and empirical outcomes.

According to ISO 14577 standard, the loading process consists of incrementally applying load over a defined period, often with a dwell time at maximum load, to establish stable contact. Unloading follows at a controlled rate after the dwell period. This standard protocol includes specimen preparation, loading/unloading cycles, data analysis, and uncertainty assessment. While it excels in providing accurate hardness and modulus measurements at the maximum load/depth reached, its quasi-static nature might limit its efficacy in capturing dynamic material responses or rapid, in-depth spatial variations.

In the following, we compare results from the three methods (high-speed nanoindentation, CSM and ISO 14577) on two representative sample materials: (a) an Al-33 wt% Cu eutectic alloy from Besharatloo et al. [23] and (b) a cement paste composite [13]. Before making any comparison, it is important to remember that high-speed nanoindentation results also depend on the method used for statistical deconvolution. Therefore, we also present a comparison of different data analysis methods for the case of the Al-Cu eutectic.

In the case of the Al-Cu eutectic, the sample's heterogeneity and co-existence of two distinct soft (aluminum) and hard (Al_2Cu) phases have been demonstrated as excellent for drawing comparative discussions on the absolute hardness and elastic modulus values as extracted from traditional grid indentation protocols based on the ISO 14577 standard and CSM. Then, we will discuss a dataset obtained on cement pastes, which represent convenient, highly heterogeneous and hierarchically structured ceramic materials whose properties depend upon several

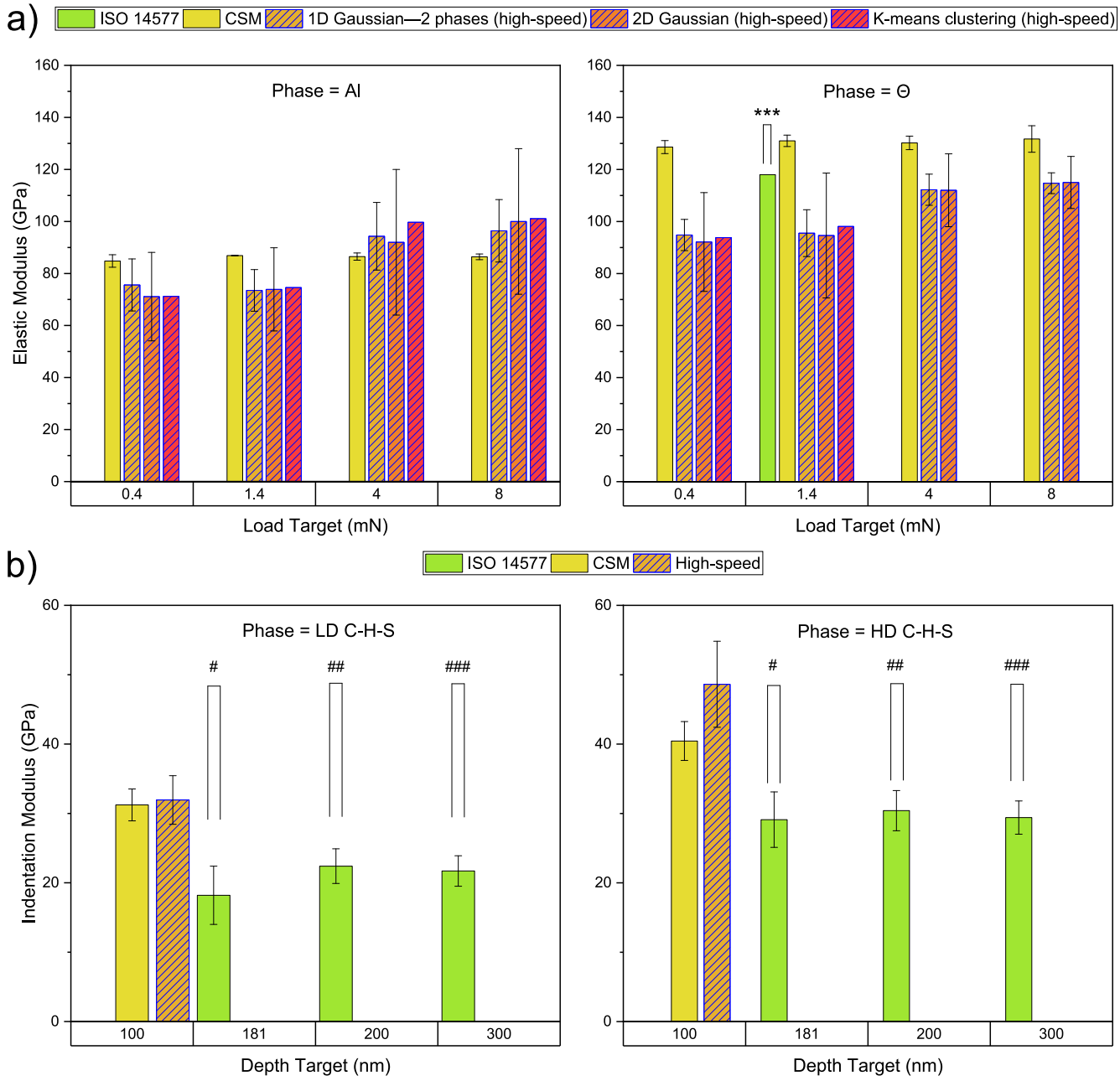

Fig. 10. Bar chart depicting differences in elastic modulus measurements across nanoindentation methodologies, loading conditions/penetration depth, and material phases for (a) an Al-Cu eutectic alloy (high-speed data from Besharatloo et al. [23]; Other literature data (i.e. refs from [38–40]) is represented, respectively, with *, **, *** symbols for readability) and (ii) cement pastes having a w/c ratio approximately equal to 0.4 (high-speed data taken from Sebastiani et al. [13]; Other literature data (i.e., refs from [6,8,10]) is represented, respectively, with ###, #, ## symbols for readability).

factors, and design strategies rely on the precise evaluation of the mechanical phase distributions.

In Fig. 9 and Fig. 10, we visually present some discussion of the main discrepancies among different testing protocols and briefly discuss their source, in view of a conscious use of high-speed mapping. In Fig. 9, the bar charts capture the relative differences in hardness values across various evaluation methods, loading conditions and literature experiments [38–40], compared with Besharatloo's data set on the same Al-Cu eutectic sample. It is important to highlight how several deconvolution methods fall under the common umbrella of high-speed mapping (evidenced in the figures via the common blue contouring and shading of corresponding bars). Indeed, single-phase properties are inevitably determined by statistical post-processing of the data via the selection of an appropriate algorithm: Besharatloo et al. have confronted three different data analysis approaches for high-speed mapping (namely, 1D Gaussian, 2D Gaussian and K-means clustering).

The complexity arising between comparing different hardness measurements becomes clear when we contrast the high-speed statistical techniques, Continuous Stiffness Measurement (CSM), and the ISO 14577 standard on the Al-Cu eutectic alloy. High-speed statistical evaluation methods offer a diverse spectrum of variations across the two different phases and loading conditions. The high-speed 1D Gaussian approach is a case in point, where hardness values exhibit substantial fluctuations within the aluminum (Al) phase. These values span from 1.87 to 2.43 GPa across distinct loads. Compared to the more confined range of 1.16 to 1.58 GPa observed in CSM and ISO 14577 measurements, this marked variance highlights the high-speed method's sensitivity to loading dynamics and the potential influence of strain rate hardening for aluminum.

In the hard phase (theta) case, the high-speed 1D Gaussian method reveals a different facet, displaying a convergence of hardness values within a narrower band, ranging from 4.84 to 6.46 GPa. This is related to the lower strain rate sensitivity that characterizes the hard theta phase. The observed hardness fluctuations for high-speed mapping can also be associated with the intricate interplay between adjacent indentations, amplifying the indentation size effect. This finding indicates that the rapid succession of high-speed methodologies could magnify spacing-dependent effects more prominently than traditional approaches. In addition, errors may arise in soft phases due to the "plasticity error", as Merle et al. and Phani et al. illuminated [41,42]. The "plasticity error" stems from the oscillatory nature of CSM tests, where the amplitude of displacement oscillation, induced by the superimposed sinusoidal load, is influenced by both the cycle's loading and unloading parts. Consequently, the contact stiffness, which depends on the ratio of load amplitude to resultant displacement amplitude, may deviate from purely elastic behavior due to plasticity error.

In parallel, the elastic modulus measurements tell a story marked by much mess pronounces discrepancies across methodologies and phases. In the Al phase, elastic modulus values span from 84.8 to 101.1 GPa in high-speed methods, while CSM presents a more compact range of 86.4 to 86.9 GPa. This divergence could partially stem from elastic modulus calculations relying on unloading behavior, rendering them less susceptible to transient influences. This divergence could also stem from the variation in contact depth and area, as discussed above, due to this dataset's high-speed load target operation.

Central to our understanding is that selecting an appropriate data analysis strategy is pivotal in high-speed methodology interpretation. The choices encompassing methodologies like 1D Gaussian, *K*-means, or 2D Gaussian have a discernible impact on outcomes. These choices can potentially intensify or mitigate the disparities observed across phases and loading conditions, introducing a layer of complexity that warrants meticulous consideration and validation.

Finally, an interesting data comparison emerges in evaluating the elastic modulus of complex cement pastes with a w/c ratio of approximately 0.4, using various nanoindentation techniques (as shown in Fig. 10-b). High-speed nanoindentation, combined with CDF data deconvolution [13], outclasses in distinguishing between various hydrated C-S-H phases in the cement. As reported in [13], conventional CSM nanoindentation fails to capture all of the C-S-H phases present in the material. At the same time, the HSNM is the only method capable of detecting the ultra-high-density C-S-H. Additionally, ISO 14577 and CSM [6,8,10], grounded in grid indentation techniques, depict lower E values, potentially owing to a limited discernment of the microstructural intricacies. Therefore, **HSNM is a powerful tool for complex multiphase (and even hierarchically structured) materials**.

2.6.1. *Standardization and reproducibility*

The provided datasets encapsulate a spectrum of hardness and elastic modulus measurements obtained through various methodologies, spanning high-speed techniques, Continuous Stiffness Measurement (CSM), and the ISO 14577 standard. These methodologies yield divergent results, raising questions about the reproducibility and comparability of measurements across laboratories and researchers.

One of the key challenges lies in establishing a standardized framework that enables consistent measurements across different techniques. By its very nature, high-speed nanoindentation introduces dynamics that differ from traditional approaches. High-speed methods' rapid loading and unloading cycles alter the indentation process's temporal and mechanical conditions. Consequently, establishing a universal set of testing parameters becomes challenging, as the essence of high-speed methods lends itself to a less uniform testing environment. To cope with this inherent variability, instrument manufacturers approach high-speed protocols by applying strategies that depend on the specific addressed hardware so that the loading and displacement time profiles are not always transparent or user-controllable. Therefore, standardization and transparency in testing parameters could represent a valuable and crucial step for comparing results obtained through different methodologies.

The complex interplay between spacing, indentation size effects, and material behavior amplifies the importance of standardization. Besharatloo et al. analysis show that indentation size and spacing concerning the length scale of a finely spaced multiphase microstructure can significantly influence the observed mechanical properties. Traditional grid indentation protocols like CSM and ISO 14577 involve larger spacing, potentially offering insulation against the spacing-dependent effects observed in high-speed methods.

In the context of the Al-Cu dataset, reproducibility is influenced by several factors. The selection of the statistical evaluation methods within high-speed nanoindentation methodologies (such as 1D Gaussian, K-means, or 2D Gaussian), as shown in Section 3 of this review article, introduces a layer of complexity that requires careful consideration. These choices can lead to variations in results, thereby impacting the reproducibility of measurements. Furthermore, selecting the maximum load or depth within high-speed methods is a critical decision to influence outcomes significantly. The continuous stiffness measurement inherent in some high-speed protocols necessitates meticulous control of these parameters to ensure reproducibility across experiments and laboratories.

Additionally, the integration of data-driven insights into these efforts is crucial. The observed trends and patterns, such as the distinct behavior in soft and hard phases, highlight the need for tailored protocols for different material types. This can enhance reproducibility by acknowledging material-specific influences and devising strategies to mitigate them.

3. Recent advances in data interpretation tools

The large amount of data generated by high-speed nanoindentation experiments can be challenging to interpret. This article section will review the most common and recently used data analysis and interpretation methods, focusing on mechanical phase analysis and recognition in nanoindentation mapping and correlation with microstructures.

These tools include statistically-aided data analysis techniques and artificial intelligence (AI)-aided algorithms, including machine learning, unsupervised clustering, and deep learning. This way, insights from nanoindentation data are extracted by identifying different material phases or regions with different mechanical properties. We will discuss each method's advantages and limitations and compare their performance.

3.1. Statistically-aided data analysis techniques

Statistical deconvolution techniques are well-established data analysis protocols for general spectroscopy, specifically for the grid and high-speed nanoindentation testing. These techniques involve separating the underlying probability distributions of different variables from a mixed dataset. Three of the most common statistical deconvolution techniques are the probability distribution/density function (PDF), cumulative distribution function (CDF), and 2D Gaussian deconvolution. PDF analysis is a statistical technique that separates the probability distributions from a mixed experimentally evaluated curve. The PDF of a variable x is defined as:

$$p(x) = (1/N)\Sigma\delta(x - x_i)$$

Where N is the total number of data points, x_i is the ith data point, and δ is the Dirac delta function.

The goal of PDF analysis is to find the best mathematical model approximating the PDF of the mixed data, p(x), and estimate the model's parameters (Fig. 11a). The most common mathematical models in PDF analysis are the Gaussian, log-normal, and Weibull distributions. One of the first and most cited articles in this field is the work by Constantinides and Ulm [8], back in 2007 and applied to grid indentation data. PDF deconvolution is a powerful technique that can provide valuable insights into the behavior of materials at the nano-scale. Still, it requires a good understanding of the underlying physics of the system and a good choice of the mathematical model. The drawback of PDF analysis is that it is sensitive to the choice of mathematical model and the estimation of the number of deconvolutional parameters.

The CDF analysis is similar to the PDF but separates the cumulative distribution functions of different variables from a mixed dataset instead of their probability distributions (Fig. 11b). The CDF of a variable x is defined as:

$$F(x) = P(X \leq x)$$

The most common mathematical models used in CDF analysis are the log-normal and Weibull distributions. Also in this case, the work by Ulm et al. [43] represents a cornerstone for the strict mathematical approach based on cumulative Gaussians applied to nanoindentation data, followed by the work of Miller et al. [11]. While less potent than PDF analysis in identifying distributions for the mechanical properties, the CDF deconvolution is less sensitive to the choice of the mathematical model than PDF deconvolution. However, it still requires a good understanding of the system's underlying physics. PDF and CDF analysis typically relies on a least square estimate of the model parameters and a minimization process between the experimental reconstructed distribution and the theoretical one.

Zhang et al., in their work on cement pastes [44], compared the two mentioned deconvolution algorithms with the Gaussian Mixture model (GMM) based on the maximum likelihood evaluation algorithm for data fitting. It is worth noting that GMM and PDF techniques are similar in their intrinsic nature (while different from a strict mathematical approach). GMM is a probabilistic model that assumes data points are generated from a mixture of Gaussian distributions. At the same time, PDF deconvolution is a technique used to remove the effects of convolution from a given distribution (and when Gaussian models are selected it approaches the GMM). The authors concluded that, for cement pastes, the calculated mechanical parameters do not vary significantly between the three tested deconvolution techniques. Still, as stated in various articles, the CDF deconvolution represents a more robust algorithm regarding covariance errors, while GMM requires a large amount of data for appropriate convergence (Fig. 11c).

2D Gaussian deconvolution is a technique that separates the underlying probability distributions of different variables from a mixed dataset in two dimensions. This technique assumes that the underlying probability distributions are Gaussian and allows probability clustering based on two mechanical outputs simultaneously (unlike the other deconvolution algorithms mentioned). The 2D histogram method has been validated for different multiphase systems, as reported elsewhere [45–47] (Fig. 12a-d), while Besharatloo's work on high-speed nanoindentation mapping represents the first consistent application to nanoindentation data [23].

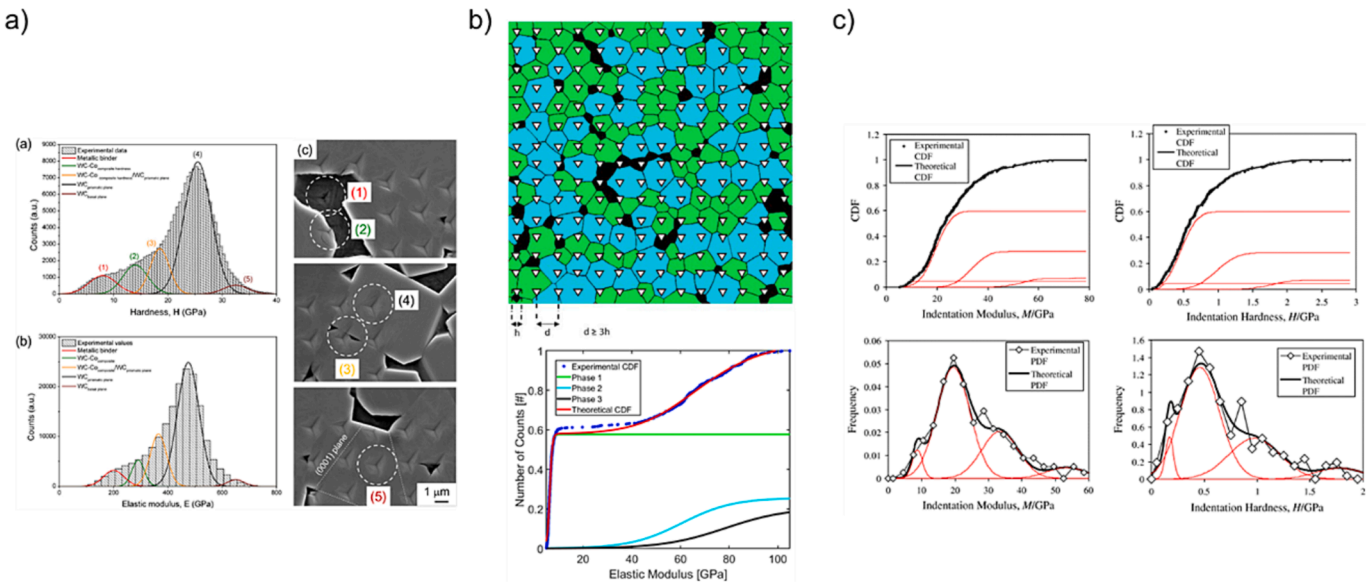

Fig. 11. Classical statistical deconvolution tools: a) PDF-based data deconvolution for phase identification WC-Co alloys (reprinted from Roa, J. J. et al. [48], Copyright(2018), with permission from Elsevier), b) CDF data deconvolution approach in multi-phase as proposed by Sebastiani et al. (reprinted and adapted from Sebastiani, M. et al. [13], Copyright(2016), with permission from Elsevier) and c) comparison between PDF and CDF deconvolution approaches as applied by on 20 by 15 nanoidentation grid on cement paste (reprinted from Ulm, F. et al. [43], Copyright(2007), with permission from Elsevier).

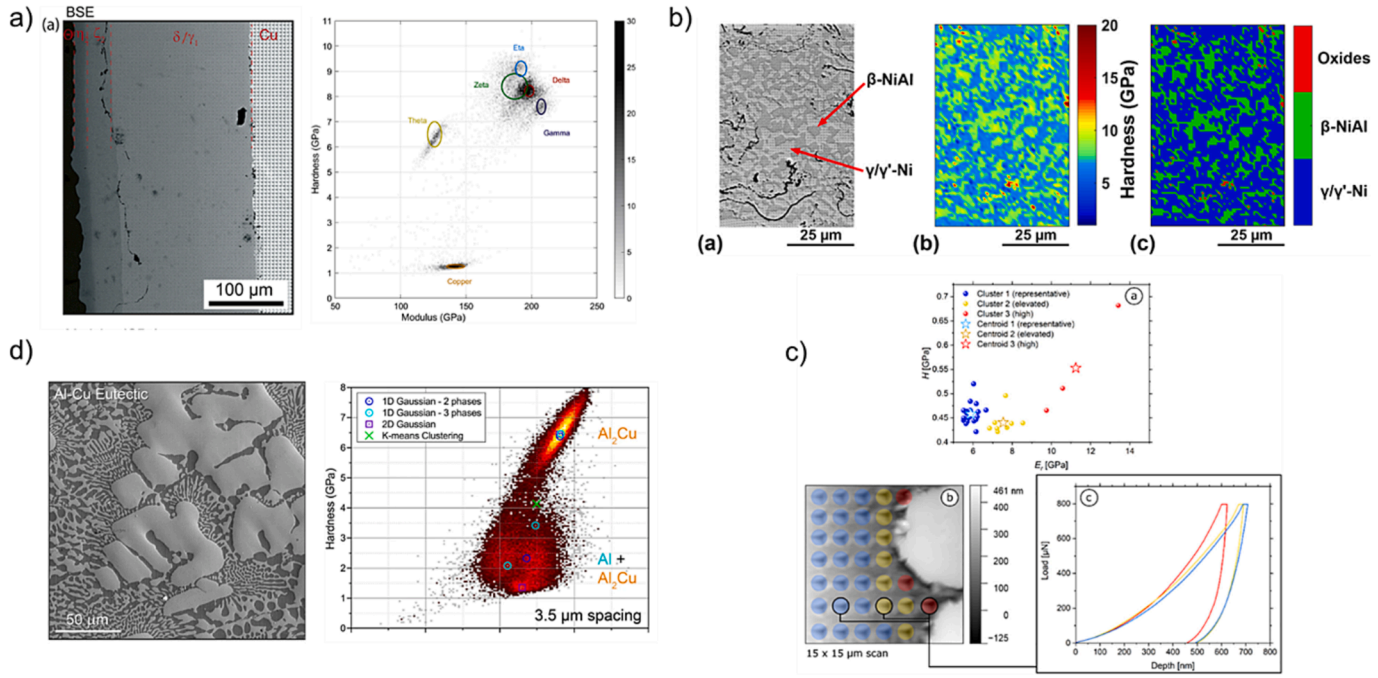

Fig. 12. Advanced blind and «Unsupervised» high-speed mapping data analysis: a) 2-D Gaussian interpolation for Al-Cu intermetallics (reprinted and adapted from Xiao et al. [47], Copyright(2020), with permission from Elsevier) and b) *k*-means clustering applied to thermal spray coatings by Vignesh et al. (reprinted from Vignesh, B. et al. [49]); c) unsupervised *k*-means clustering for organic matter-rich rocks with identification 1:1 correlation of load-depth behavior (reprinted from Vranjes-Wessely, S. et al. [52]) and d) comparison between phase-identification efficiency on Al-Cu eutectic alloy of classical blind statistical analysis and advanced deconvolution techniques as a function of indent spacing (reprinted and adapted from Besharatloo, H. et al. [23]).

3.2. *Artificial intelligence (AI)-based deconvolution techniques*

Artificial intelligence (AI) is a branch of computer science that deals with developing systems that can perform tasks that typically require human intelligence, such as visual perception, speech recognition, decision-making, and language understanding.

In nanoindentation, AI-based techniques have been used to analyze the large amount of data generated by nanoindentation experiments. These techniques can be used to identify different material phases or regions with different mechanical properties, which can provide valuable insights into the behavior of materials at the nano-scale. AI techniques can be broadly classified into rule-based systems and machine learning.

Machine learning (ML) is a subset of AI that enables systems to learn from data and make predictions or decisions without being explicitly programmed. ML algorithms can be divided into supervised, unsupervised, and reinforcement learning. In supervised learning, the algorithm is trained on a labeled dataset and learns to predict the output for new inputs. In unsupervised learning, the algorithm is not provided with labelled data, and it has to discover the underlying structure of the data on its own. Reinforcement learning is machine learning in which an agent learns to make decisions by interacting with its environment. In high-speed nanoindentation unsupervised data clustering algorithms are widely used to establish a spatial and statistical correlation between mechanical data and phases within heterogeneous tested systems.

3.2.1. *Data clustering techniques*

Among all the unsupervised learning techniques, clustering is often a common choice. *K*-means is one of the most widely used clustering algorithms. It partitions a dataset into *k* clusters, where the mean of the data points in that cluster represents each cluster position in the variables space. The algorithm iteratively assigns each data point to the cluster with the closest mean, then updates the clusters' means. In nanoindentation, *k*-means can be used to group similar indentation test results, which can help to identify different material phases or regions with different mechanical properties. However, the *k*-means algorithm is sensitive to the initial conditions and can sometimes converge to a local minimum instead of the global optimum. The first work to consistently apply *K*-means algorithms for mechanical phase recognition in nanoindentation data is by Koumoulos et al. on constituents phase reconstruction of a mortar surface trough grid nanoindentation [50], while the work by Vignesh et al. represents this review's first application on high-speed nanoindentation data (as detailed in the following sections and Fig. 12b-c) [49].

K-medoids are a variation of *k*-means that uses the medoid, the most centrally located point in a cluster, instead of the mean to represent the cluster. *K*-medoids are more robust to noise and outliers than *k*-means, but it is also computationally more expensive.

Another popular clustering technique is hierarchical clustering, which creates a hierarchical tree-like structure to represent the nested clusters in the data. In this method, the data points are iteratively merged or divided based on similarity until a stopping criterion is met. Hierarchical clustering can be represented in two forms: agglomerative and divisive.

Another popular unsupervised clustering technique is DBSCAN (Density-Based Spatial Clustering of Applications with Noise), which forms clusters based on the density of data points. This algorithm can discover clusters of arbitrary shapes and is robust to noise and outliers.

In conclusion, unsupervised clustering techniques such as *k*-means, *k*-medoids, Hierarchical Clustering, and DBSCAN are powerful tools for data analysis in nanoindentation. They can be used to identify different material phases or regions with different mechanical properties, which can provide valuable insights into the behavior of materials at the nano-scale. The choice of technique depends on the specific problem and the characteristics of the data.

These techniques have been recently detailed by Sousa et al., highlighting how said approaches can be applied, their limitations, and the need for data pre-processing before clustering and statistical analysis [51].

3.2.2. Deep learning techniques

Deep learning is a subset of machine learning that uses deep neural networks to learn representations of data automatically. These models are trained using large amounts of data and can learn complex, non-linear data representations. Deep learning algorithms have achieved state-of-the-art performance in various tasks, such as image and speech recognition, natural language processing, and gaming. Some of the most common deep-learning techniques applied to nanoindentation data include:

1 Artificial neural networks (ANNs) are layers of interconnected artificial neurons that process and transmit information. The network is trained using a dataset, where input data is presented to the network, and the network's output is compared to the desired output. Based on this comparison, the network's parameters are adjusted to minimize the difference between the output and the desired output. Once trained, the network can make predictions or decisions based on new input data without being explicitly programmed.
2 Convolutional neural networks (CNNs) have the same building structure as the ANNs. Differently from them, the basic building block of a CNN is the convolutional layer, which applies a set of filters to the input data, creating a feature map. Additional layers then process this feature map to extract higher-level features from the data. Once trained, CNN can classify novel knowledge based on its learned features.
3 Recurrent neural networks (RNNs) comprise interconnected artificial neurons that can retain information from previous time steps, allowing them to analyze data more contextually. RNNs are well-suited for natural language processing, speech recognition, and time-series prediction tasks. They have been applied to nanoindentation data to identify temporal patterns.
4 Generative models such as Generative Adversarial Networks (GANs) and Variational Autoencoders (VAEs) can be used to generate new nanoindentation data similar to the original data.

Supervised clustering has been recently reviewed as a promising tool for informed categorization of data [53], with specific application on the identification of material responses for fiber–matrix interfaces in composite materials design (Fig. 13b). Moreover, convolutional neural networks (CNNs) to analyze nanoindentation mapping data are particularly interesting. As a practical example, Kosmann et al. [54] used a CNN to analyze nanoindentation mapping curves behavior and identify hidden information within the elastoplastic response of ceramic coatings, aluminum alloys, fused quartz, and silicon to enable pop-in identification. CNNs, indeed, are particularly well-suited for image analysis tasks.

Finally, deep learning techniques have also been used to analyze nanoindentation data in combination with traditional statistical deconvolution techniques, such as probability distribution function (PDF) and cumulative distribution function (CDF) analysis. This approach uses deep learning algorithms to extract features from the data and then uses these features to perform a more detailed analysis using traditional data analysis techniques. An example of this is the work by Bianco et al. [55], where the authors used a deep neural network to rectify incorrect experimental spatial measurements acquired during nanoindentation modulus mapping (as shown in Fig. 13a), reducing uncertainty in materials' properties using state-of-the-art computer vision techniques.

3.3. Comparison between different data analysis techniques

In the previous sections, the most popular data deconvolution techniques employed for analyzing gird and high-speed nanoindentation datasets have been briefly reviewed and contextualized within the latest and most prominent works in the literature. However, choosing the most suited algorithm for mechanical phase extraction relies on each methodology's specific problem and the mathematical and theoretical hypothesis. Above all, one of the main driving forces for any algorithm is effectively removing outliers within the analyzed dataset. Within a high-speed mapping experiment, outliers, adding onto measurement errors and calibration errors, can occur for several reasons:

1. Surface defects: if the material's surface contains defects, such as cracks or pores, this can lead to outliers in the data.

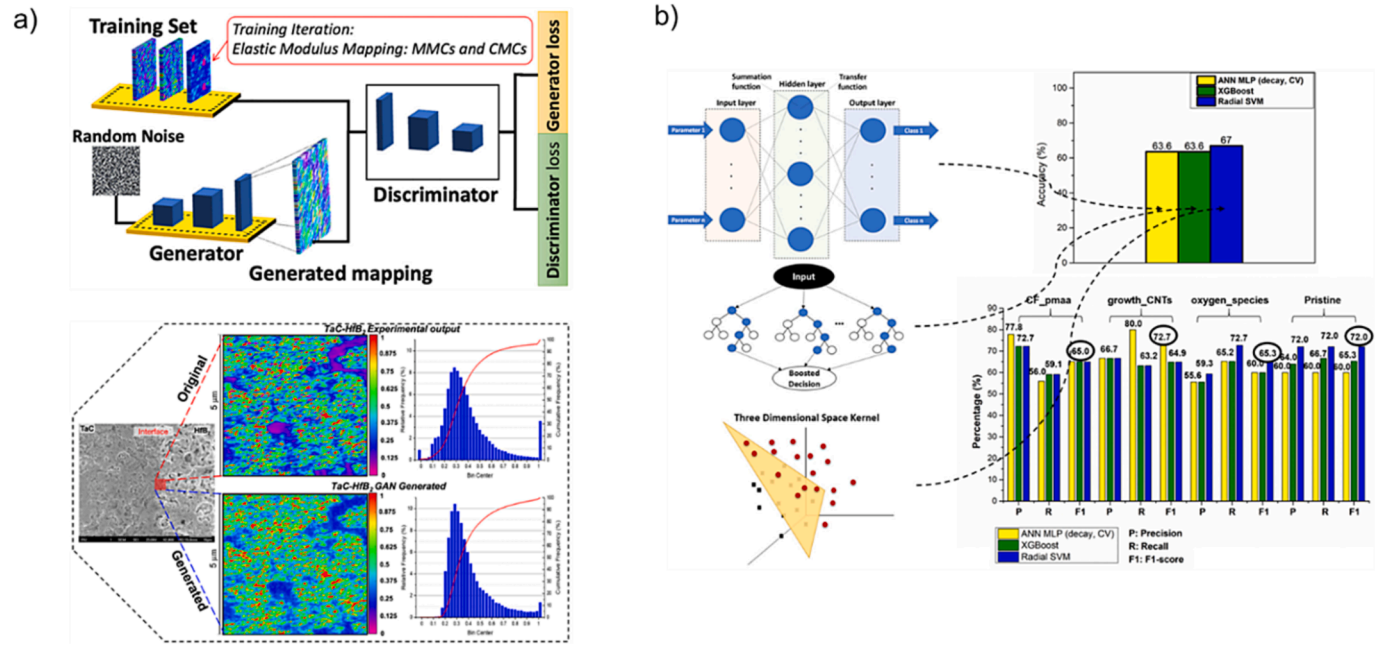

Fig. 13. Supervised deep-learning and machine learning approaches to high-speed nanoindentation mapping: a) deep-learning applied to PDF statistical deconvolution for data-filtering and adaptive reconstruction of nanoindentation data (reprinted from Bianco, G. et al. [55], Copyright(2022), with permission from Elsevier); b) comparison between different approaches for supervised clustering (reprinted from Konstantopoulos, G. et al. [53]): Artificial Neural Networks, Extreme gradient boosting and 3D Space kernel.

2. Sample preparation: the sample preparation process can also lead to outliers. For example, if the sample is not adequately cleaned or has not been sufficiently prepared for nanoindentation.
3. Rapidly varying inhomogeneities: some materials may have inhomogeneities, such as grain size or composition variations, which can lead to outliers in the data when an indentation test occurs at the interface of two mechanical phases.
4. Non-linear behaviors: some materials may exhibit non-linear behavior, such as plastic deformation or phase changes, which can lead to outliers in the data.

PDF and CDF algorithms, while being useful to understand the statistical robustness of the deconvoluted phases within a material as an outcome of the mapping process, may not be as effective for identifying complex relationships (also requiring for initial hypothesis on the numerosity of the distributions to be deconvoluted) or when dealing with large amounts of data. Additionally, assumptions on the underlying model distribution of data are needed as insights into the physical phenomena by which those distributions arise.

On the contrary, clustering algorithms are well suited for discovering new relationships within the data. A great advantage relies on retaining the spatial position of each data point within the clustering process, making it possible to elaborate mechanical phase maps. However, Euclidean distance minimization patterns can be sensitive to the initial conditions, the number of clusters specified in advance, and outliers.

Deep learning algorithms are particularly well-suited to identify patterns and trends in nanoindentation data, overcoming most drawbacks of the previously mentioned methodologies. However, deep learning requires extensive data to train the networks and can be computationally intensive.

Overall, for complex data analysis algorithms to be applied in the deconvolution process of high-speed nanoindentation data, a crucial step in data pre-processing is necessary to filter out most of the issues described in Section 2 of this review. Approaches based on evaluating spurious contributions to the stiffness measured in each test location have been developed over time, analyzing the statistical distributions of mechanical properties derived from un-filtered data and single load-depth behaviors from depth-sensing indentation (Continuous Stiffness Measurement). One of the first rigorous approaches to high-speed nanoindentation data pre-processing and filtering is proposed by Amanieu et al. [15], shown in Fig. 14, demonstrating the protocol on complex heterogeneous $LiMn_2O_4$ particles, carbon black, and PVDF embedded micro-constituents in a compliant epoxy matrix. The proposed protocol consists of a two-step process that evaluates non-quadratic load versus displacement curves in the nanoindentation response and filters out data diverging from the hypothesis underlying the Oliver and Pharr methodology of an isotropic semi-infinite sample [2]. Typical non-quadratic responses arise from inter-phase borders or cracking of the tested material. A 2-order polynomial fit function is fitted on the load–displacement curves discarding the Hertzian spherical contact occurring at the very first nanometers of the interaction. The second step consists of a comparative evaluation of the compliance of the contact in comparison with the applied load: the Joslin-Oliver parameter [56], considered to be constant for a contact in a semi-infinite space (without mixed contributions), is evaluated for each indent and a threshold slope (for which mixed contributions are sought to be present in the elastic modulus evaluations) is defined; tests that are above this threshold are automatically discarded.

However, in some cases, load–displacement curves are unavailable in high-speed mapping due to the massive amount of data that needs to be stored otherwise. In those cases, statistical analysis could consider filtering out outliers based on convolutional methods of PDF distributions in an iterative fancy.

4. Correlative mechanical microscopy

The successful design of novel materials and devices at the micro- and nano-scale requires a thorough understanding of the complex relationships between microstructural features (surface and bulk), production processes, and performance [57]. High-speed nanoindentation mapping provides fast, statistically reliable, and highly spatially-resolved information on the mechanical properties of materials at the nano-scale. However, it cannot provide direct information on the material's local crystal structure and orientation, chemical composition, and surface topography. Often, the relationships between local mechanical properties and these structure/composition parameters are of most interest to materials scientists.

As outlined in the previous section, various analysis approaches are available to extract these relationships and identify trends in the data. However, the robustness of these statistical analysis approaches – such

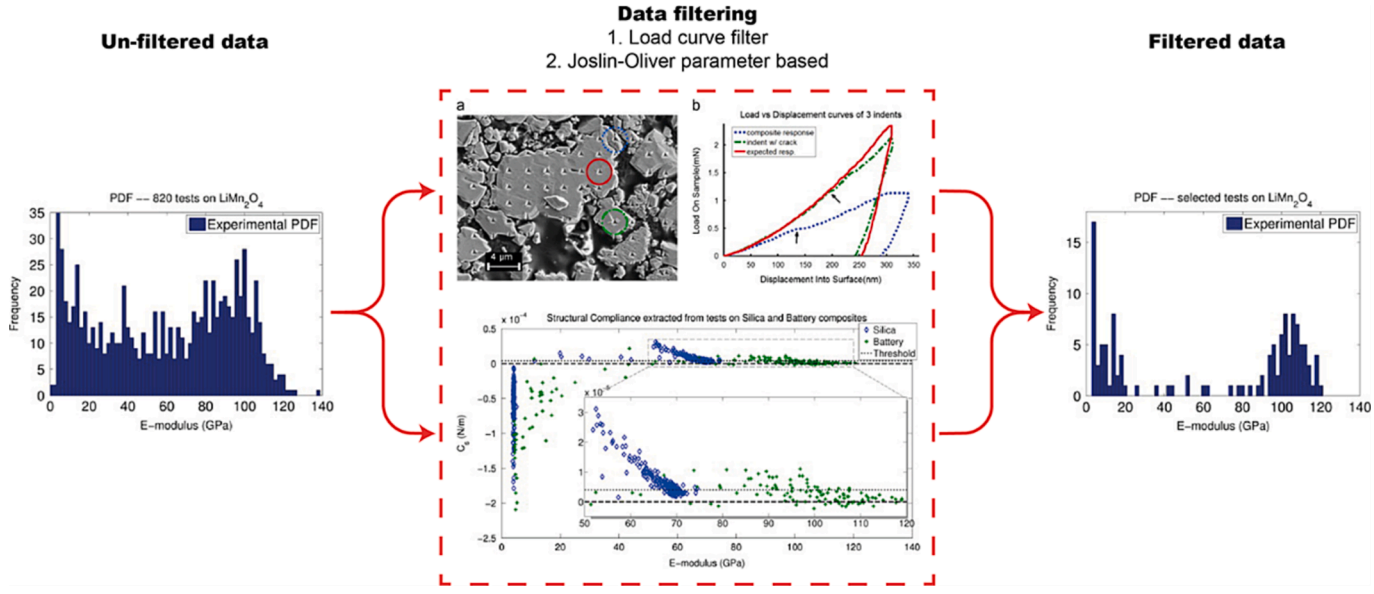

Fig. 14. Data filtering strategy for PDF and CDF deconvolution algorithms for high-speed in-depth nanoindentation data based on load curve behavior filtering and structural compliance Joslin-Oliver parameter as described by Amanieu et al. (reprinted and adapted from Amanieu, H.-Y. H. Y. et al. [15], Copyright(2014), with permission from Elsevier).

as PDF, CDF, machine learning-aided cluster identification, and other relevant data categorization techniques – often requires additional modalities to add extra dimensions to the data to aid in the convergence of mathematical problems behind classifying or segmenting the data, especially when property changes are continuous within a microstructure.

Multi-dimensional datasets can be robust for identifying microstructural features such as grain boundaries, precipitates, or phases. This allows them to provide additional layers of understanding of microstructure-properties relationships.

With this premised, a straightforward approach to performing comparative analysis consequently derives from a visual comparison between the areal data from the different informative techniques employed. As the prominent strategy for comparative mechanical microscopy, the **visual correlation** is a **qualitative analysis approach** where the visual features or patterns in two datasets are compared to identify similarities or differences. Generally, a visual correlation would involve qualitatively comparing the indentation patterns with, for example, crystallographic or elemental maps to identify any relationships or correlations. Visual correlation primarily relies on a qualitative comparison of the patterns, features, or trends visible in the datasets. It generally involves visually inspecting the nanoindentation maps alongside other techniques (e.g., EBDS or EDX maps) to identify similarities, discrepancies, or potential correlations. Image correlation techniques are often applied for a precise, qualitative overlap of the plots. While informative for qualitative observations, it does not provide accurate quantitative information about the relationships between the datasets. This comparative approach, as described, has been widely applied so far to a variety of materials research topics where informed microstructural and mechanical analysis is needed to identify spatially localized data patterns: advanced steels testing, 3D printed metals, multi-phase alloys, etc., of which the most prominent and cutting edge application will be reviewed in Section 5.

The term **correlative microscopy strictly refers to cases involving data registration**. In this circumstance, the multi-technique informed analysis consists of a **numerical alignment and merging of the different datasets** obtained from the various measurement techniques or instruments. In the context of high-speed nanoindentation maps, data registration refers to the process of quantitatively aligning, via data analysis and domain transformation operations, the indentation data with the corresponding maps obtained via different techniques, considering and retaining the different spatial resolutions attaining to each data set and aligning the related spatial locations.

This numerical alignment enables quantitative analysis and precise correlation between the datasets. It involves domain transformation methods, where mathematical translations, rotations, scaling, or deformations are employed to align the datasets accurately. These transformations are typically based on features or markers present in both datasets. Once the datasets are aligned, data registration enables the quantitative analysis of indentation parameters (e.g., hardness, modulus) concerning, for example, the crystallographic or elemental information obtained from EBSD or EDX maps.

Accurate registration between different modalities can be challenging, as various imaging techniques have different resolutions/sampled volumes and inherent distortions. The main issues that prevent correct registration of the maps include:

- Sample deformation: the sample may deform during imaging, resulting in different deformation patterns over the techniques employed.
- Inherent distortions: different imaging techniques have inherent distortions that must be corrected for accurate registration. Section 2 of this review highlights many prominent inherent errors and distortions affecting a nanoindentation map. Additionally, EBSD is mainly affected by intrinsic errors in detector geometry, errors due to the high angle between the detector and the primary diffracting beam, and aberrations in beam shape.
- Resolution differences: The resolution of the different imaging techniques may vary, leading to the misalignment of the maps. The resolution of nanoindentation tests mainly depends on various factors, including the hardness and elastic modulus of the material itself, the depth of indentation, the shape of the indenter tip, etc.

The very first data registration approach for informed elemental and nano-mechanical analysis applied to high-speed nanoindentation mapping data refers to the work of Wheeler [45] where 1:1 EDX-nanoindentation map correlation has been achieved for each data point in Cartesian space in which, contrary to traditional elemental registration strategies on grid indentation involving smooth compositional gradient fitting with mathematical functions describing the gradients [47,58,59].

Subsequently, a notable work on this topic proposes the exact approach for multi-modal map registration, aiding the correlation between high-speed nanoindentation and several analytic electron microscopy techniques, particularly EBSD and WDS [60] - Fig. 15a. While the specific steps and derived limitations in multi-technique map registration are detailed in Magazzeni et al., the main steps behind multi-modal correlations are summarized here. An essential step in the registration process is defining “fiducial parameters” for a first tentative registration between maps. Then affine geometric transformations are performed on the acquired data to align the spatial coordinates of the multi-variable/multi-modal domain space in which a single *n*-dimensional correlation function can be extracted. This serves as a direct correlation means between the multiple datasets. Several filtering strategies are adopted – as virtual reconstructions of crystallographic data or interim statistical analysis – to strengthen the correlation function’s reliability while removing outliers. This finally results in clear mechanical properties trends with crystallographic orientation to be revealed (Fig. 15a), highlighting the potential of the multi-modal approach.

Another notable work in correlative nanoindentation and electron microscopy by Wilson et al. [61] utilizes the elemental analysis capabilities of energy-dispersive X-ray spectroscopy (EDS). While it was developed using standard grid indentation methodologies rather than HSNM, it is worthy of mention in this section for its development of an automatic protocol for nanoindentation and quantitative EDS (NI-QEDS), specifically designed to determine cement and cement paste properties at the micro- and nano-scale level. The NI-QEDS methodology is based on specific Monte Carlo-trained spectral investigations at each indent position, via precise translation of locations onto the same ROI in the SEM to be used as input for the EDS acquisition software. This NI-QEDS analysis enabled chemical phases with strongly overlapping mechanical properties to be clearly distinguished (Fig. 15b).

These two notable examples illustrate the ability of correlative HSNM to extract mechanical properties as a function of structural or chemical parameters.

5. Recent case studies and applications

Throughout this review, it has been evidenced how high-speed nanoindentation mapping has become a game-changing technology for spatially-resolved nano-scale mechanical analysis in advanced materials with complex structure–property relationships. These materials systems include advanced composites, 3D printed metals, multi-phase alloys, and natural hierarchically-architected materials (e.g., wood, bone, nacre). This section focuses on the recent and most relevant applications of high-speed nanoindentation mapping to these systems and highlights how this technique can be an enabling technology. A significant role of HSNM is shown to be revealing hidden features that affect mechanical properties, such as grain size, porosity, defects, and heterostructures, ultimately helping to optimize the design and performance of

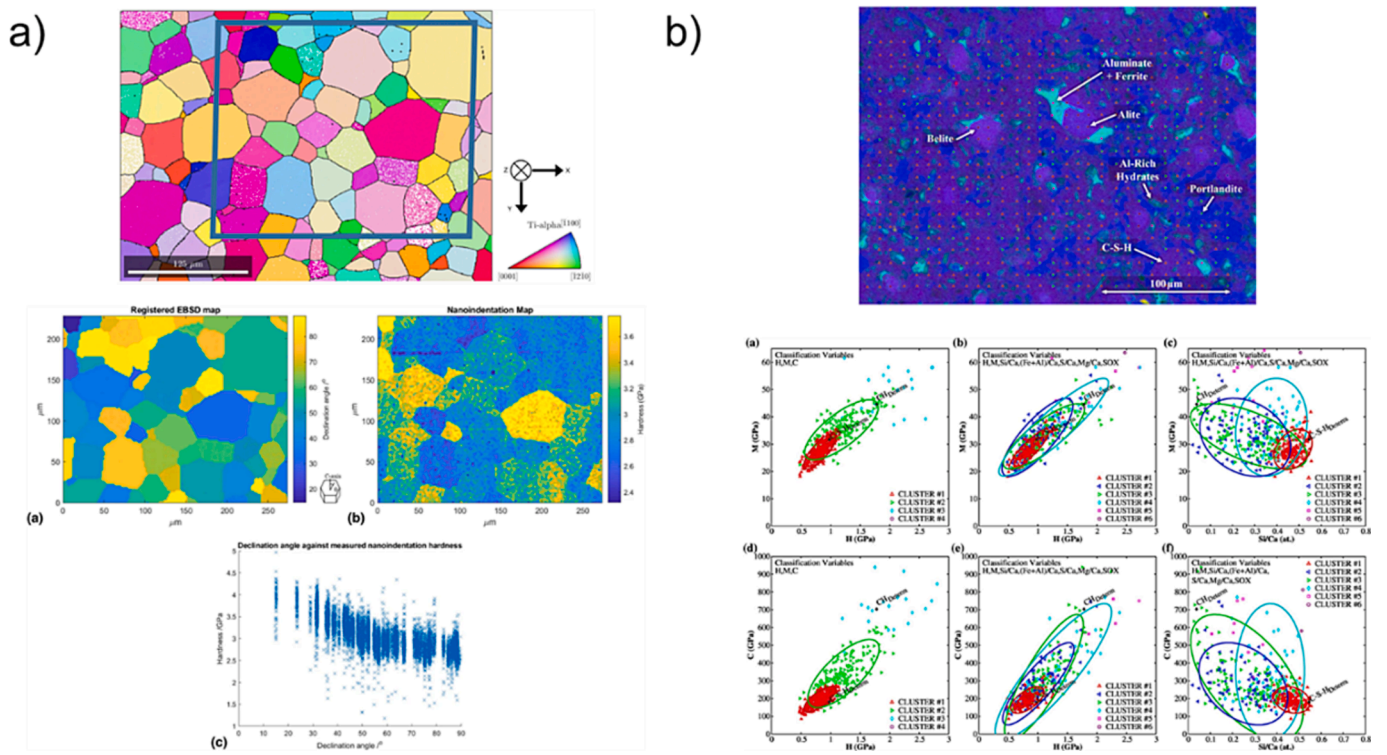

Fig. 15. Examples of high-speed data interpretation improvements via EBSD mapping correlation: a) multi-modal maps combinations for registration and correlation of high-speed data and EBSD analysis in CP titanium (reprinted and adapted from Magazzeni, C. M. et al. [60]), b) NI-QEDS automated classification method of phases based on a correlative approach between mechanical data from nanoindentation and point-to-point correlated EDS measurements applied on cement pastes (clustering approach evidenced, reprinted and adapted from Wilson W. et al. [61], Copyright(2018), with permission from Elsevier).

materials in various critical applications, including aerospace, automotive, energy, civil constructions, and biomedical engineering.

5.1. Additively manufactured metals

Additive manufacturing (AM) has revolutionized the manufacturing industry by enabling the production of complex geometries and structures that were once difficult or impossible to create using traditional manufacturing techniques. Metals are becoming increasingly popular among the various materials that can be additively manufactured due to their unique properties and broad applications. However, they exhibit microstructural heterogeneity and mechanical anisotropy, affecting their performance and reliability [62]. Therefore, understanding their microstructural and mechanical properties is essential for optimizing the processing parameters and predicting their behavior under various loading conditions.

Microstructural and mechanical characterization of AM metals should involve the analysis of their crystal structure, grain size, porosity, defect density, and mechanical properties such as strength, ductility which are strongly influenced by the printing parameters, such as the laser power, scanning speed, layer thickness, and build orientation [63]. Additionally, knowledge of the microstructural and mechanical properties can aid in developing new materials, optimizing design parameters, and validating printing simulation models. High-speed nanoindentation has been described in the previous sections as the key point application whenever complex mechanical information over large areas is of interest: its application on AM components is a natural derivation of its intrinsic characteristics, given the need for this specific manufacturing field.

Correlation with EBSD, SEM, and EDS is generally fundamental when analyzing microstructural features from AM-manufactured metals. Specifically, information from EBSD is often used to understand: (i) interface structures between voxels and crystalline habits after cooling, (ii) microstructural evolution during post-processing of the 3D printed structures. It is essential to understand the microstructural evolution during the printing and cooling of 3D LPBF or SLM metallic parts, for which EBSD is a crucial investigation tool.

At the same time, nanoindentation provides a fundamental analysis of mechanical properties' evolution from the skin to the core of filament extruded samples. To this scope, the seminal work of Gardner et al. [64], which posed attention to titanium alloys oxygen embrittlement and combined EBSD analysis, EPMA, and high-speed nanoindentation to investigate the complex relationship existing between oxygen concentration, microstructure, crystal orientation, and hardness.

Liu et al. [65] were the first to use advanced techniques to study the microstructures and mechanical properties of Ti-6Al-2Zr-Mo-V alloys made through additive manufacturing. They found correlations between mechanical properties (hardness and elastic modulus) and phase differences (α and β) and examined the effects of heat treatment. The *k*-means clustering algorithm was used to analyze the nanoindentation dataset, **visually** relating mechanical property maps to the distribution of α and β phases determined by EBSD mapping. The study also identified a clear mechanical profile of the α/β boundaries, essential for understanding local deformation mechanisms. By combining high-speed nanoindentation mapping with XRD, BSE, and EBSD characterization (Fig. 16a), the researchers measured the distribution of hardness and elastic modulus near the α/β boundary, enabling analysis of micro-shear bands in LDED near-alpha alloys under different heat treatments [66].

On the same track, Shakerin et al. [67] studied the interface engineering of additively manufactured maraging steel-H13 bimetallic structures for which the excellent printability and weldability – promising for fabrication of load-bearing components in the aeronautical industry – is hindered by the inhomogeneous microstructure across the interface that can degrade the performance of bimetallic components in service conditions. The authors used EBSD to analyze the microstructure and crystallographic orientation of the materials and high-speed

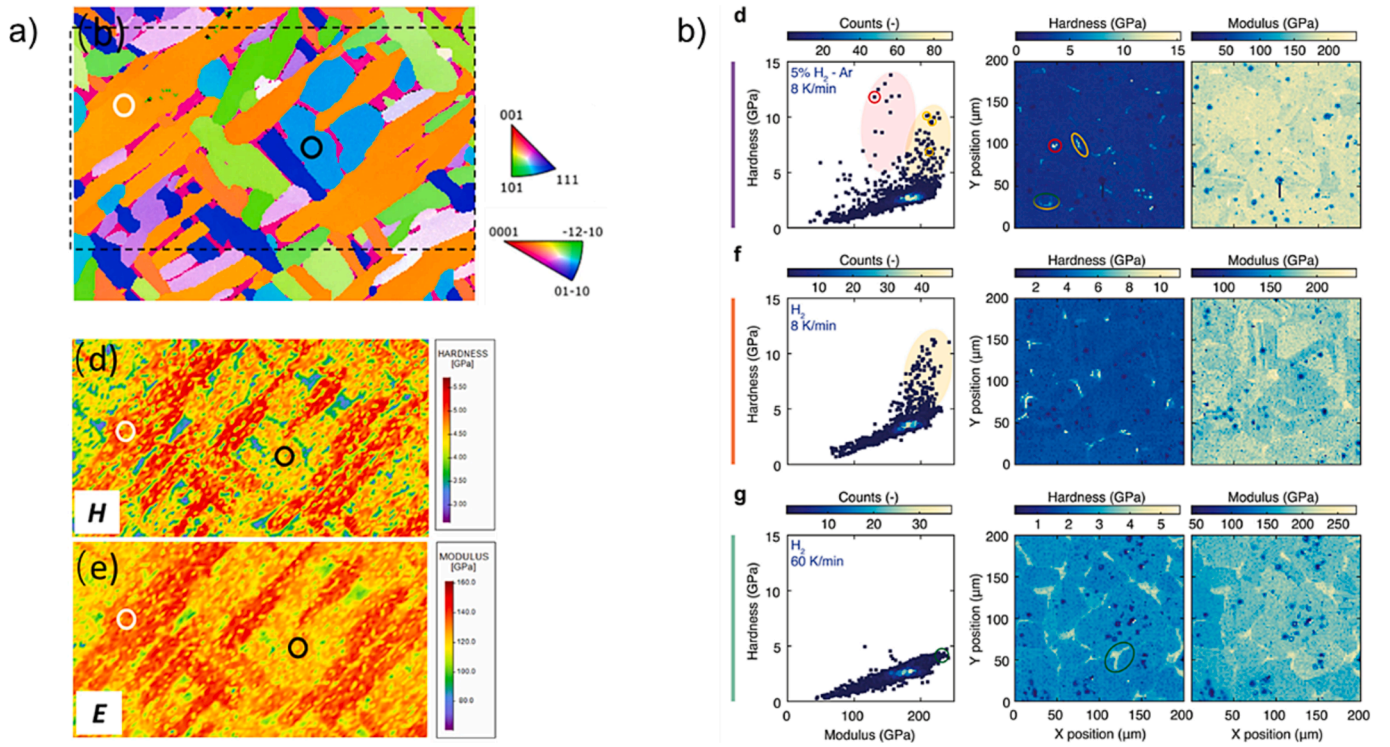

Fig. 16. Representative examples of high-speed nanoindentation mapping in AM metals: a) correlation of mechanical properties with microstructural changes during heat-treatment of 3D printed Ti alloys (reprinted and adapted from Liu, Z. et al. [65], Copyright(2021), with permission from Springer Nature); b) phase identification in 316 filament extruded steel as a function of atmospheric conditions: Cr-Mo-rich phase correlation (adapted from Wagner, M. A. et al. [68]).

nanoindentation to determine the mechanical properties and behavior of the interfaces between the two materials. The correlative analysis allowed them to understand the structure–property relationship at the interface, which is essential for designing and optimizing bimetallic structures.

Other than beam-based metal AM techniques, which have been reviewed in the previous paragraphs, an innovative study by Wagner et al. [68] studies filament extrusion-based additive manufacturing as an alternative. A relevant problem to the industrial implementation of this FDM fabrication process is commonly the need for post-processing (sintering) of the structures to achieve the final product (while rapid solidification processes determine beam-based techniques microstructures). It is essential, therefore, to investigate how the sintering process (temperature, cooling rate, atmosphere) affects the overall performance in terms of densification, microstructures, and phase formation (hard precipitates are detrimental to mechanical reliability). EBSD and EDX measurements provide partial information on the elemental distribution due to diffusion and the resulting microstructures. The interplayed role of these elements in determining the final tensile properties along with quantification of the porosity could be only studied by coupling the information with high-speed nanoindentation, allowing not just to determine the best printing parameters (the authors found that high sintering temperatures of 1350 °C, an atmosphere of pure H_2, and a cooling rate of 60 K/m resulted in the optimal microstructure, with high densities and no hard phases that could negatively impact mechanical properties) but also detrimental phases such as pores, -ferrite, spinel oxides, and precipitates were easily identified in the indentation data from various sintering conditions (Fig. 16b).

5.2. Advanced alloys

Advanced alloys such as steel and high-entropy materials enhance sustainability and performance in high-end applications. These materials offer superior mechanical properties, corrosion resistance, and thermal stability, enabling the development of lighter, more durable, and energy-efficient structures [69].

Developing higher strength and durability steels can reduce the steel needed for a given application, resulting in lower energy consumption and emissions. Obtaining microstructural-informed properties is essential for designing high-performance materials that can withstand extreme conditions. Therefore, a modern goal for material scientists is to characterize, model, and design microstructural features, such as grain size, morphology, hard phases distribution and shape, and crystallographic texture, that could play a critical role in enhancing structural reliability with achieving an adequate balance with deformability.

Duplex stainless steels represent a notable starting point in that sense. Small-scale characterizations for this class of steels are scarcely available compared to macro-scale investigations. The distinct mechanical behavior between austenite and ferrite leads to some damage and failure (edge cracks), ultimately demanding studies of the plastic compatibility between the constitutive phases. Besharatloo et al. [46] addressed this problem, debating on how HSNM, while being a suitable means of investigation, is insufficient for performance characterization at the micro-scale in these steels (and for other similar contexts) due to the instability of phases due to different factors and the presence of alloying elements and specific processing conditions that could lead to the austenite and ferrite showing relatively similar mechanical properties. There's a strong need for correlative microscopy in which phases are priorly determined by microstructural characterization techniques (EBSD).

A notable application of high-speed nanoindentation and EBSD/EDX mapping for advanced steels investigates the most prominent issues for structural applications: stress corrosion cracking in welds, specifically, chloride-induced stress corrosion crack propagation in an austenitic stainless-steel weld [70]. EBSD was used to analyze the crystallographic orientation and microstructure of the material and high-speed

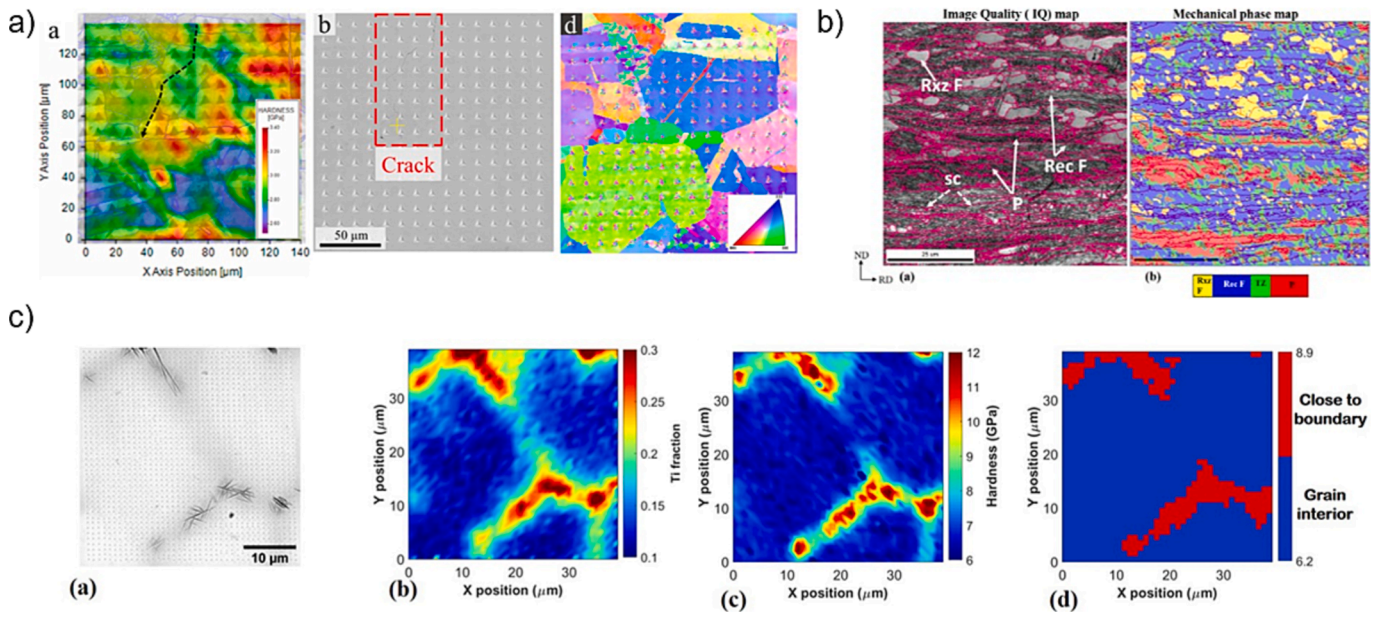

Fig. 17. Examples of high-speed mapping in advanced alloys (from steels to complex HEAs): a) chloride-induced stress corrosion cracking in austenitic stainless steel (adapted from Qu, H. J. et al. [70]), b) recrystallization behavior in proeutectoid steels (reprinted and adapted from Janakiram, S. et al. [71], Copyright(2021), with permission from Elsevier), c) effect of chemical segregation on the local mechanical properties of multi-principal element alloys (reprinted and adapted from Kalali et al. [72], Copyright(2023), with permission from Springer Nature).

nanoindentation to determine the mechanical properties and behavior of the material under stress. The correlative analysis allowed an understanding of the relationship between the microstructure and mechanical properties of the material under chloride stress corrosion cracking conditions (Fig. 17a).

Another relevant work on the microstructural evaluation of advanced steels in correlation with their mechanical properties at a multi-scale understanding level is reported by the work of Janakiram et al. [71], in which the authors investigated the early recovery kinetics in ferrite-pearlite cold-rolled high-strength sheet steels. The study's objective was to understand the early stages of recovery in the material after cold rolling. How it affects the mechanical properties, to which scope, by coupling complementary techniques such as high-resolution nanoindentation mapping and electron microscopy (EBSD and TEM), microstructure-property correlations at the micrometer length scale (shown in Fig. 17b) were established to provide new insights on the driving force for temperature and composition-dependent recovery kinetics.

High entropy or multi-principle-element alloys are metallic alloys with four or more elements near equiatomic ratios. These alloys have demonstrated unique combinations of high strength, ductility, and corrosion resistance, which has generated significant research interest in recent years. However, designing and optimizing entropy alloys for specific applications requires a thorough understanding of their microstructure and mechanical properties at the micro- and nano-scale levels. Therefore, chemical and mechanical analysis techniques to achieve the desired distribution of chemical elements (avoiding elemental segregation/phase separation) are vital to the final performance. To the authors' knowledge, the recent work from Kalali et al. [72] represents the first work that combines correlative EDS and high-speed nanoindentation with the specific objective of designing MoNb and MoNbTi HEAs, providing a simple framework to study the effect of chemical segregation on the local mechanical properties of multi-principal element alloys (as shown in Fig. 17c). The work of Meghwal et al. represents another valuable research on the topic [73] in which the authors not just studied microstructural evolutions in HEAs via microstructurally-informed high-speed nanoindentation mapping. Still, they transferred the knowledge base of indentation protocols to HEAs coatings, with the initial aim of observing anisotropic mechanical deformations at the local level while providing correlation with the grain structure and the overall response for the bulk.

Of the reviewed works on high-entropy alloys, the authors would focus, as a final and informative example, on a novel work that transferred statistical analysis, microstructural-informed (correlative), and mechanical properties mapping into the field of designing novel HEA materials all at once to understand a metastable transformative HEA with a chemical composition of $Fe_{38.5}Mn_{20}Co_{20}Cr_{15}Si_5Cu_{1.5}$. Dhal et al. [74], indeed, succeeded in enabling multifaceted insights into the complex hierarchical and heterogeneous deformation mechanisms of the particular HEA analyzed, therefore providing a basis on how to apply high-resolution nanoindentation mapping augmented with machine learning-based clustering, ultimately understanding dislocation activities during indentation, gamma transformations and GMM clustering for mapping and classifying the work hardening and phase dependency of mechanical behaviour.

5.3. *Composite materials*

Composite materials, defined as consisting of two or more distinct phases combined as a matrix and a reinforcement to produce a material with enhanced properties, possess peculiar microstructure-property-performance relationships mainly determined by the type, volume fraction, and orientation of the reinforcement phase, as well as the characteristics of the matrix phase. By selecting and controlling the properties of constituent materials, composite materials can be tailored to meet specific performance requirements, such as high strength, stiffness, toughness, or thermal conductivity. To this extent, it has been crucial for researchers to understand the spatial distribution of mechanical properties in the constituent phases, interfaces, and their intertwined role, along with defects distribution, in determining local failure modes and overall structural performances. It is worth mentioning that HSNM on composite materials characterized by significant differences in the elastoplastic response between the reinforcement and the matrix poses a relevant challenge, specifically in load-control indentation, related to differences in the probed volumes over hard or soft phases and, therefore, specific optimization routes to avoid

overlap during testing. Three notable application clusters are identified and discussed in this section: (i) cement and cement pastes, (ii) cermets, (iii) ceramic matrix composites, and (iv) in polymer-matrix composites.

5.3.1. Cement and cement composites

As discussed in the introduction of this review, the microstructure of cementitious materials comprises different phases, including cement clinker, hydration products, and aggregates. Cement paste is a highly complex material with numerous phases, including calcium silicate hydrate (C-S-H), calcium hydroxide (CH), and other minor phases. These phases contribute to the cement paste's strength, stiffness, and other mechanical properties. Therefore, it is crucial to assess microstructural features of these individual phases, such as the size and morphology of the particles, the distribution of the pores, the chemical composition, and the evolution of the hydration products with time. High-speed nanoindentation of cement pastes and cementitious materials primarily aims at determining the mechanical properties of various phases as a function of parameters such as the water/cement ratio, the addition of nanoparticles, and the microstructural composition. As mentioned previously, seminal works in using grid quasi-static indentation by Constantinides and Ulm [6,8], were in this field, exploring the effects of two types of C-S-H on the elasticity of cement-based materials. Sebastiani et al. [13] performed the first work that systematically employed high-speed nanoindentation mapping to identify hydration products during the ageing of cement pastes, aided via correlative EDS measurements.

On the same track, and in comparison with grid indentation, Němeček et al. [75] validated high-speed nanoindentation mapping protocols on three different cementitious materials representing blended cement and other composites with a higher level of heterogeneity than Portland cement, as studied by Sebastiani's work (Fig. 18a). Results were compared qualitatively and quantitatively to quasi-static indentation, highlighting remarkable agreements of values while identifying critical issues in those phases (specifically hydrated ones) where strain rate effects may be prominent.

5.3.2. Cermets

Materials science often attempts to perform micro-structural optimization via data analytics over the relevant length scale of the interactions between the different phases. However, in cermets, macroscopic length scale mechanical properties have historically been reported with little information on the micro-scale behaviors. The first seminal work by Roa et al. [48] in the field employing high-speed nanoindentation in combination with microstructural characterization techniques (EBSD crystallographic analysis) studies the correlation between microstructure and mechanical properties at the nanometric length scale of individual WC grains, as well as the metallic cobalt binder in WC-Co cemented carbide systems, providing novel information on the local mechanical response at interfaces between ceramic particles with different orientations as well as regions within the metallic cobalt binder close to the WC-Co interface. Besharatloo et al. [76] applied high-speed nanoindentation to investigate, in Ti(C,N)-FeNi systems to analyze the distribution of the two main constitutive phases (the metal matrix and the Ti(C,N) particles), their distribution and the amount of porosity as a function of the ceramic/metal phase ratio. It was also possible to evaluate hardness over multiple length scales, not only focusing on the microstructure but also probing gradients within the two distinct phases themselves. PDF analysis provided average values for each constitutive phase, opening up the evaluation of properties variations in cermets as related to the specific influence of microstructural/processing variables, e.g., carbon addition or ceramic/metal phase ratio on phase level properties.

5.3.3. Ceramic matrix composites

Similarly to cermets, HSNM enables correlation of structure–property relations in ceramic matrix composites. An excellent example of this is the nanoindentation studies performed on carbon nanofibers for SiC composites (SiC, SiC-CNF) by Mubina et al. [77], where more than 10,000 indents allowed hardness and elastic modulus values of individual phases from the maps to be correlated with the microstructure of the samples. Also in this case, HSNM allowed the measurement of small variation in the properties of the phases within the sample, as well as the interface properties between the fiber–matrix and surface coating-substrate matrix, and the identification of uniform and dense columnar-structured CVD SiC coating with a cubic structure as having superior mechanical properties. HSNM was demonstrated as a successful tool for monitoring of complex relationships existing between the binder, interphase regions and overall microstructural assemblage.

This was also shown in the work of Gordon and co-authors [78] for

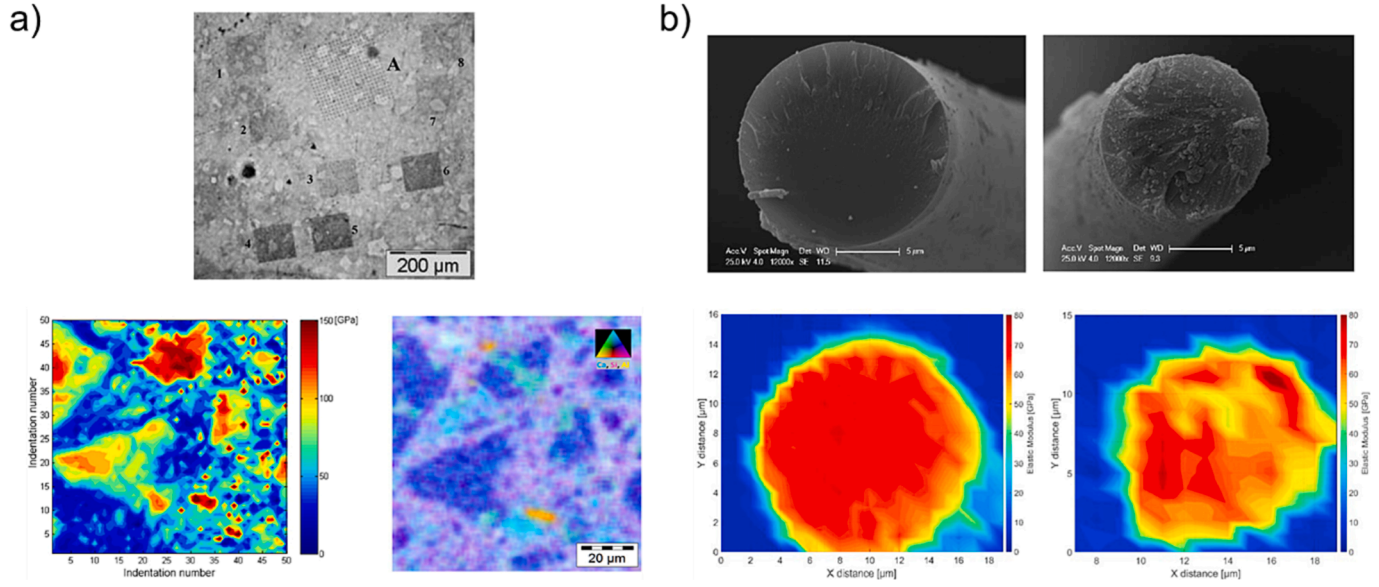

Fig. 18. High-speed mapping of cement pastes and polymer matrix composite materials: a) identification of C4AF clinker phases, the yellow to C3S clinker phase as a function of the hydration time (reprinted and adapted from Sebastiani et al. [13], Copyright(2016), with permission from Elsevier), b) damage evolution in basalt fibres cross-sections as a function of the recycling temperature (reprinted and adapted from Lilli et al. [79], Copyright(2020), with permission from Elsevier). (For interpretation of the references to colour in this figure legend, the reader is referred to the web version of this article.)

three different grades of polycrystalline cubic boron nitride (PcBN) composites, where the use of binders for cBN sintering is crucial to reduce the range of temperatures needed and improve the mechanical performance. PcBN is mostly used in cutting tools and as a replacement for superalloys and hardened steels. HSNM coupled with 1D and 2D gaussian deconvolutions for average phase properties recognition was shown to be the only method that allows study of such information at the relevant microstructural length scales for PcBN. For the purposes of this review, a crucial finding is represented by the reported differences between 1D and 2D gaussian deconvolution of mechanical phases for small grain size and/or binder mean free path phases. In such cases, 1D Gaussian fitting achieved the best results.

5.3.4. Polymer matrix composites

Polymer-matrix composites pose significant challenges for HSNM due to the large differences in the elastic–plastic response of the reinforcement and matrix. In this area, two relevant works apply HSNM to investigate the evolution of sub-micron scale mechanical properties in the reinforcement phase and the overall distribution of strains and stresses due to the coupling of these two main constitutive phases.

Lilli et al. [79] used HSNM to identify local clusters in mechanical properties over cross-sections of recycled Basalt fibers to understand the damage (Fig. 18b), damage localization, structural reorganization, and crystallization as a function of the thermal treatment process leading to their recycling process. High-speed nanoindentation enabled a new understanding how thermal treatments lead to a loss of tensile properties with thermal cycling temperature due to local variation of mechanical properties on the surface of the fibers. Quasi-static measurements could only evidence average properties over the whole fiber in correlation with fracture toughness.

Irez et al. [80], on a similar path, drew attention to an important impact of high-speed nanoindentation for polymer-matrix composites characterization and design: the evaluation of the mechanical interaction between reinforcement phases and polymer binder along with the quantification of their distribution within a representative surface area (for randomly oriented particles). In their work, the authors studied scrap rubber powder fillers optimized through boron and alumina addition. High-speed nanoindentation was performed to evaluate the stress distribution between the hard-ceramic particles and the polymeric binder. In contrast, PDF distribution analysis was employed to understand the homogeneity of the dispersions.

5.4. Thin and thick films

This chapter delves into the distinct realms of thin and thick film testing, terms derived from the films' physical dimensions and the technologies employed in their deposition. Thick films, generally ranging in thickness from a few micrometres to millimetres, are developed through thermal and plasma spraying processes, resulting in materials with pronounced heterogeneity and porosity. These characteristics necessitate high-speed mapping nanoindentation to rapidly assess mechanical properties and phase compositions, a crucial step in optimizing designs for applications like thermal barrier coatings. Conversely, thin films, with thicknesses spanning nanometers to a few micrometres, are fabricated through refined techniques such as atomic layer deposition (ALD) and magnetron sputtering. These films enhance biocompatibility and boost electrochemical and wear performances in emerging technologies by adding nanofillers or realising complex micro- and nano-architecturing [81]. The chapter further explores the pivotal role of deconvoluting substrate effects during high-speed testing of thin films. It is essential to accurately determine their mechanical properties and foster advancements in biomedical devices and wear-resistant coatings.

5.4.1. Thick films: Sprayed coatings

Sprayed coatings are relatively thick depositions used in large industrial components to provide wear, thermal, and corrosion protection. Due to the nature of the technologies employed for production, the mechanical properties of these coatings are influenced by their heterogeneous microstructure that includes splat boundaries, porosity, interface between layers, and cracks. High-speed nanoindentation mapping is employed to identify, categorize, and mechanically model the individual and composite response of the heterogeneous microstructural features that could be found and identify peculiar features that may form or develop as a function of the operating conditions.

5.4.1.1. Cermet coatings. One of the relevant studies on sprayed coatings in the literature by Suresh Babu and co-authors [82] focuses on WC-Co coatings for abrasion and erosion resistance. This work aimed at understanding the relationship between the microstructure and properties present in the feedstock powders and the coatings themselves (upscaling to the whole final product the information from the raw materials). In this application, HSNM (in Fig. 19a applied on the cross-section of WC-$(W,Cr)_2C$-Ni particle) proved important to characterize the degradation of the mechanical properties as a function of the harsh environmental parameters in which these technologies are envisaged to work. This provided insights into the development of wear and corrosion products and mechanical changes in the initial phases present: cumulative hardness distribution profiles evidenced differences for several production parameters. HSNM clarified the differences in plastic response between the WC phase and the $(WCr)_2$ matrix, variations in the Cr content for the matrix itself, and formation of Ni-Cr matrix, while the deconvolutions provided a means of understanding the overall performances.

5.4.1.2. Thermal barrier coatings. Several efforts with HSNM have been made on thermal barrier coatings (TBCs) in sprayed coatings, which are fundamental to energy production and transportation. TBCs are widely used to protect metallic components in high-temperature applications, such as gas turbines, diesel engines, and aerospace systems. These coatings typically consist of two or three layers, including a metallic bond coat, a ceramic topcoat, and occasionally a ceramic interlayer. The ceramic topcoat is the primary component of TBCs, which serves as the first line of defense against the high-temperature environment. The typical ceramic materials used in TBCs include yttria-stabilized zirconia (YSZ), gadolinium zirconate (GZO), and other rare-earth oxides. These materials have excellent thermal insulation properties, low thermal conductivity, and high melting points. The thickness of the ceramic topcoat ranges from a few microns to several hundred microns, depending on the application requirements.

Historically, grid nanoindentation [83–85] has been utilized to evaluate the effects of thermally-induced microstructural changes and severe oxidative environments – as a function of the coating's deposition technique – on single micro-constituents of the TBCs. This aimed to understand possible in-service mechanical performance degradation due to the development of tensile residual stresses at interfaces or within the top coat. Researchers were interested in the properties of the top coat and its degradation as the primary source of failure. A primary reason for TBC failure is the development of a thermally-grown oxide (TGO) layer at the interface between the ceramic topcoat and the metallic bond coat, formed due to the oxidation of the metallic bond coat during service. Grid nanoindentation was applied to assess TGO growth mechanisms and evolution with thermal cycling.

Two main considerations reveal the importance of HSNM in the field of TBCs: (i) the coating's microstructural heterogeneity requires large numbers of indentations to reveal the complex intertwined contributions to the overall mechanical robustness of the coating; (ii) the thermal cycling-dependent nature of the evolution of these micro-constituents also requires large numbers of indentations with high lateral resolution. The development of HSNM represented a valid and essential tool for understanding the overall response of a TBC coating as a function of

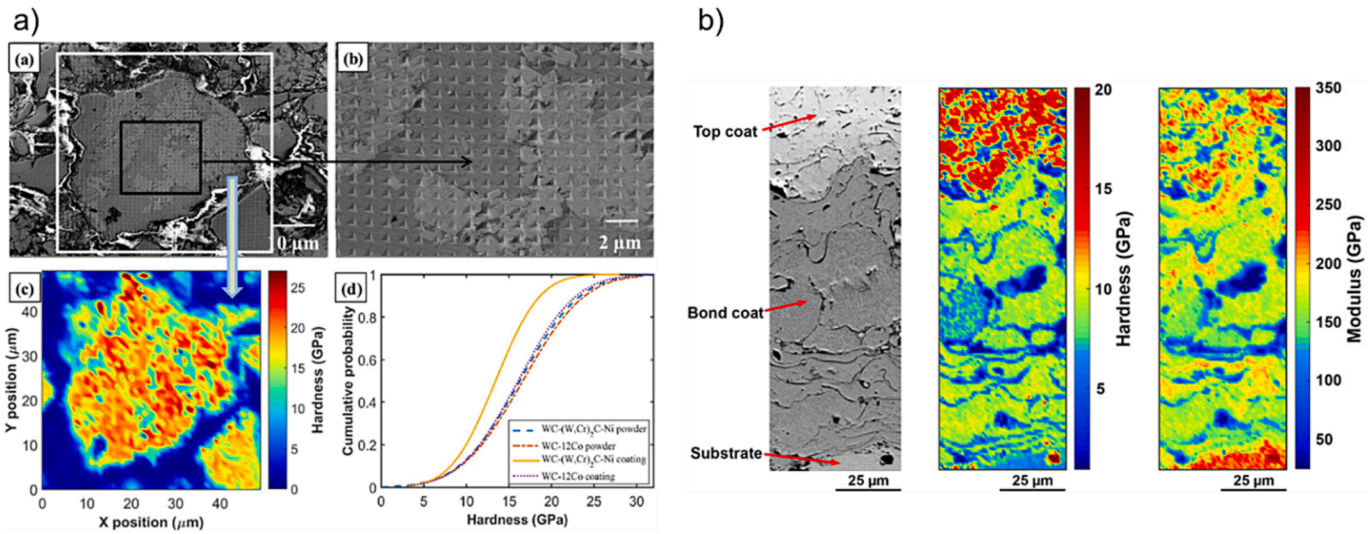

Fig. 19. a) Nano-indentation array on the cross-section of WC-$(W,Cr)_2C$-Ni with cumulative hardness distribution profiles of powders and detonation sprayed coatings (reprinted from Babu et al. [82], Copyright(2018), with permission from Elsevier), and b) high-speed nanoindentation along the cross-section profile of a thermal barrier coating to study the evolution of the whole substrate-coating system during thermal cycling (reprinted from Vignesh et al. [49]).

thermal cycles and in the presence of heterogeneous phases and cracks. The main advantage of high-speed nanoindentation is the possibility of performing large area maps. This aids in identifying gradients of mechanical properties from the bond coat to the top surface of the coating and in understanding the distribution of mechanical phases and the evolution of the TGO (and its impact on the in-service performances). Two main studies applying HSNM to thermal barrier coatings are reviewed.

Using high-speed nanoindentation, Bolelli et al. [86]. investigated the damage progression in TBCs during thermal cycling. The authors performed a depth-sensing high-speed nanoindentation mapping on a TBC system consisting of a NiCrAlY bond coat and a YSZ topcoat. The indentations were performed on as-deposited samples and samples thermally cycled at 600 and 800 °C. The authors observed a significant increase in the indentation depth and crack length after thermal cycling at 800 °C, indicating the initiation and growth of cracks in the ceramic topcoat. The authors also observed a decrease in the elastic modulus and hardness of the ceramic topcoat after thermal cycling, which could be attributed to the microstructural changes and damage accumulation in the TBC system. Moreover, the high-spatially resolved mechanical data evidenced a growth of the thermally grown oxidized with cycling temperature, which, after development above a critical threshold, was determined to become the primary source of the developed cracks.

Vignesh et al. [49] boosted the importance of high-speed nanoindentation of heterogeneous complex coatings testing addressing the evolution of the mechanical properties as a function of the thermal cycling focusing on deconvolution techniques for mechanical phase identification. The authors used high-speed nanoindentation to map the mechanical properties of a TBC system consisting of an MCrAlY bond coat and a GZO topcoat (SEM images of the indented area and corresponding mechanical properties maps are presented in Fig. 19b). The authors observed a variation in the mechanical properties of the TBC system across the sample, which could be attributed to the non-uniformity of the microstructure and composition of the TBC system. A decrease in the elastic modulus and hardness of the ceramic topcoat near the TGO layer is reported, indicating the weakening of the ceramic topcoat due to the TGO layer's growth. The accuracy of the data deconvolution methods was systematically addressed. They found its dependence on several factors, including the number of indents, the depth of the indents, and the presence of residual stresses in the coatings. The authors also proposed an improved data deconvolution method based on *k*-means unsupervised clustering, which, as discussed in Section 3, preserves the spatial distribution of the identified mechanical phases.

5.4.2. *Thin films testing: Substrate effects in high-speed mapping*

Thin films are crucial in various industries, including microelectronics and protective coatings, requiring detailed mechanical analysis to maintain their functional efficacy. However, their mechanical testing through nanoindentation is often a complex process. As the thickness of the film decreases, the substrate's influence becomes a significant factor, demanding sophisticated methods to determine the film's true mechanical properties accurately.

Substrate effects originate from the complex interplay between the elastic and plastic properties of the film and the substrate during indentation testing. The pioneering framework established by Doerner and Nix (1986) has been vital in outlining these effects [87], underscoring the importance of isolating substrate influences to identify the inherent properties of the films correctly. Subsequent research has expanded on this foundation, developing analytical models grounded in finite element simulations and experimental data to precisely measure the mechanical characteristics of thin films [88,89]. These models consider various factors, including the disparity in the elastic modulus and the phenomena of pile-up or sink-in around the indenter, which is discernible through the evaluation of contact stiffness to the indentation depth and film thickness.

Continuous Stiffness Measurement (CSM) has emerged as an indispensable tool in this domain, facilitating the continuous gathering of stiffness and hardness data to depth, thus providing a thorough understanding of the material's response to indentation. CSM enhances the efficiency of the testing process and creates avenues for the effective implementation of analytical models, enabling a detailed analysis that accurately discerns the films' intrinsic mechanical properties by mitigating substrate effects. Hay and Crawford (2011) developed a composite response model that leverages Continuous Stiffness Measurement (CSM) to obtain contact stiffness as a continuous function of penetration depth [90]. This approach enables the discernment of the substrate-independent modulus of thin films, even at increased depths, thereby facilitating a more nuanced understanding of their mechanical properties during nanoindentation testing.

The application of high-speed nanoindentation mapping in thin film testing is a relatively unexplored territory in existing literature. While testing generally involves using a soft film on hard substrates and limiting penetration depths to a tenth of the film thickness to minimize

the substrate's impact on hardness measurements, a significant gap remains in high-speed mapping for thin films. In the burgeoning field of micro- and nano-architected films, high-speed methods that integrate CSM modes, a feature increasingly available in recent testing protocols and equipment for high-speed testing (e.g., NanoBlitz 4D), are particularly promising, allowing for the real-time application of deconvolution models during the high-speed mapping process and thereby directly achieving a properties map with reduced substrate effects. Still, the gap stems from a limited understanding of the interconnected roles of strain rate effects and plastic zone constraints, limited user control of testing parameters – such as indentation strain rate, CSM oscillation frequencies and amplitudes, etc. (as discussed in Section 2.6.1) – coupled with the absence of a rapidly applicable deconvolution method for extensive 4D datasets (encompassing x, y, hardness/elastic modulus, and depth).

5.5. Natural materials

Natural materials are substances that occur in nature and have not been, or to a minimal part, artificially processed by humans, such as biological structures or minerals. They are often comprised of various organic and inorganic components that interact with each other to form complex structures. Cellulose, lignin, keratin, hydroxyapatite and minerals, along with their higher-degree structures, are remarkable examples for this class. One of the defining features of natural materials is their structural and mechanical heterogeneity which generally encompasses exceptional performances. This heterogeneity arises from the complex interplay between the various components, which vary in size, shape, and properties, which can result in variations in the mechanical and structural properties of the material at different length scales and is achieved through the specific environmental conditions for their formation and, in most cases, over hundred thousand years of adaptation and optimization processes. This refers to the fact that they are composed of different components that vary in size, shape, and properties. Understanding the nature of this heterogeneity is crucial for predicting their behavior under different environmental and loading conditions to (i) envisage novel fields of application that could benefit from the intrinsic sustainability of natural materials or (ii) develop novel material systems with improved performance and functionality that mimics or implement those characteristics. High-speed nanoindentation is a crucial tool to these scopes, given its intrinsic connotation as a statistical tool that allows the quantification of these heterogeneities over large areas.

5.5.1. Wood

One of the most prominent fields of HSNM application examines cellular heterostructures of wood and wood cells that represent a natural composite material for which gaining information is crucial for biomasses processing and high strength-to-weight ratio structural applications. Within the field, a significant limitation is represented by the poor lateral resolution and deficiency in discrimination of traditional quasi-static indentation testing behaviors. Qin et al. [91] and Klímek et al. [92] investigated these local variations using high-speed indentation mapping for the first time. These studies allowed characterization of the presence of chemical composition gradients and ultrastructures of different cell wall layers, which contribute, along with the micrometer length-scale heterogeneity, to the structural efficiency of wood; The compound middle lamella (possessing measurably lower reduced modulus values: nanoindentation mapping showed that the elastic modulus of the cell wall around the middle lamella was about 64% of the value at the location attributed to the S2 layer within the cell wall) that links two adjacent wood cells the key revelation to the mechanical reliability. This was used to develop and better tune the properties of structural adhesive joining biomasses.

Indeed, wood products are often engineered in a higher degree of composition materials like laminates and strand boards employed in civil wooden architecture for which the wood-adhesive interfaces have been determined to play a crucial role. Xu et al. [93] showed HSNM as a tool to understand adhesive infiltration and interphase formation (as shown in Fig. 20) highlighting the importance of gradients in the distribution of mechanical properties of wood-phenolic resin (wood-PF) and wood-polyurethane (wood-PUR) interphases with the mechanical properties of the cell wall increasing due to adhesive infiltration. HSNM was also applied to reveal the mechanical performance of the early wood-adhesive interphase, which cannot be characterized by commonly used quasi-static methodology due to its small size (for which precise alignment could only be achieved statistically).

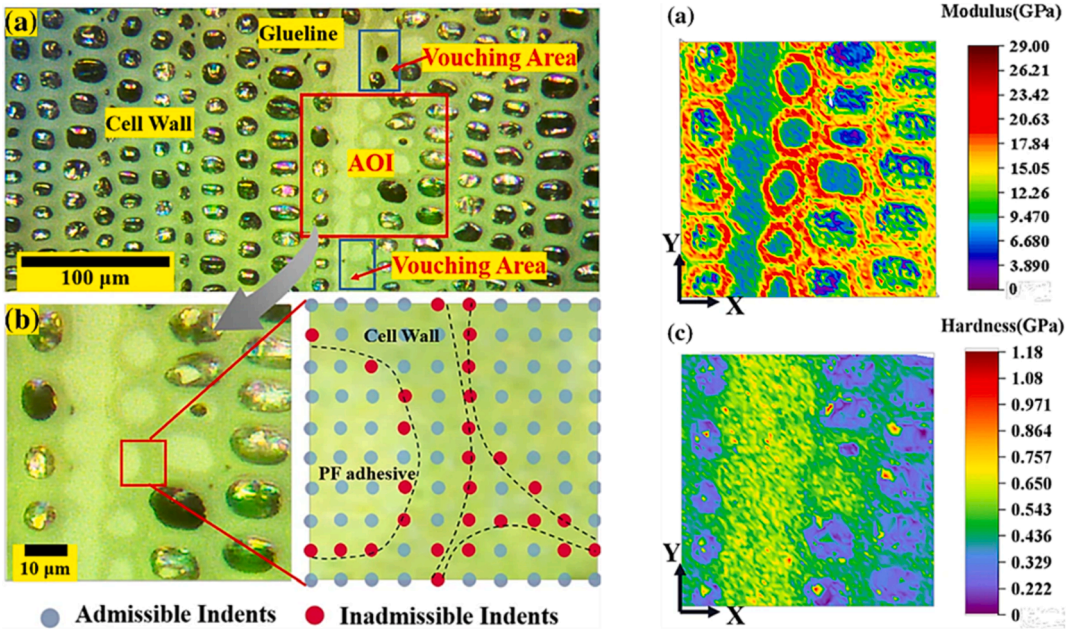

Fig. 20. Example of HSNM to assess wood cell-walls properties as a function of wood adhesive percolation (reprinted and adapted from Xu et al. [93], Copyright (2022), with permission from Springer Nature).

5.5.2. Meteorites

At this point, it will be apparent to the reader that high-speed nanoindentation is mainly intended, in natural materials studies, to highlight the relationships between the distribution of the phases that form complex heterogeneous structures and the final performances of the material itself. This information is, indeed, mainly inaccessible to quasi-static indentation due to the poor lateral resolution of grid positioning. On the contrary, given a large number of indents, high-speed nanoindentation increases the probability of tracking small phase distributions in large and fast maps. This concept is comprehensively demonstrated in the work of Wheeler on Ni-Fe meteorites [45], in which HSNM has been employed to map the mechanical properties and composition of the Taza meteorite (see Fig. 21a): a Plessitic Octahedrite nickel–iron meteorite (officially designed as NWA 859). The meteorite has a microstructure called the Widmanstätten structure. The study involved mapping ~100,000 indentations to statistically determine the properties of the individual phases of the meteorite. Five microstructural phase were characterized, and mechanical phase identification was confirmed using EDX measurements. The author achieved the first direct, point-to-point correlation of EDX and large-scale indentation maps in this study and the first measurement of the mechanical properties of the Tetrataenite ($FeNi''$) and the Cloudy Zone ($FeNi'' + Kamacite$ nanocomposite) phases. Mechanical phase maps showed superior phase contrast to EDX in two phases. An indentation property map or a mechanical phase map using a 2D histogram was used to visualize and statistically characterize the phases and identify relationship trends. The study extends the finding to the potential optimization of nickel–iron superalloys by mimicking hetero-structures formed in the Taza meteorite.

5.5.3. Minerals

Moreover, heterostructures in minerals are not merely scientifically fascinating; they also have critical industrial applications. Zircon, in particular, is a mineral studied extensively for its potential use in nuclear waste management. However, to the authors' knowledge, until the advancement in high-speed mapping, the correlation between mechanical damage progression due to irradiation and microstructural elements in nuclear-resistant minerals is very scarce and backs to the first nanoindentation measurements. The varying crystallinity content of micro-lamellar structures formed in zircon due to extensive exposure to different nuclear radiation intensities has been studied by Beirau et al. [94] where nanoindentation high-resolution mapping served as a unique tool to investigate the mechanical properties of a natural, highly zoned zircon crystal, which has variations in U and Th concentrations resulting in a range of α-decay event doses (banded structure in optical micrography shown in Fig. 21b). The study found that the directly measurable stiffness^2/load provides a valid estimate of the degree of radiation damage (as visible from the correlation between the mechanical properties maps, the banded microstructure and degree of crystallinity spectrum: Fig. 21b). At the same time, correlation with fracture toughness measurements evidenced a close correlation between toughening mechanisms and amorphization due to radiation damage as only exploitable by mapping [95]. Overall, the study provides insights into the effects of radiation damage on the mechanical properties of zircon and highlights the importance of considering heterogeneous damage distribution in designing materials to immobilize plutonium.

As further proof of the postulate that considers, in this review, high-speed nanoindentation as the only suitable probing technique for the intrinsic heterogeneities in minerals, and natural materials in general, with the solid intention for designing energy carriers materials and nuclear waste disposal technologies, Varnjes-Wessely et al. [52] employed HSNM to study the properties of natural composite materials such as shales and organic matter-rich rocks. This work aimed to find alternatives to standard macroscopic measurements, which provided low precision and inconsistent results without any capability to map the individual component. The complexity of these materials makes it challenging to extract representative material parameters such as reduced elastic modulus and hardness for organic matter. The study focuses on extracting representative hardness and elastic modulus values for organic matter in an over-mature sample set from the Chinese Songliao Basin and evaluating the influencing factors of these parameters. HSNM and machine learning techniques were used to process the results. The study found that the inherent heterogeneity of organic matter is responsible for the considerable scatter in previous data. In

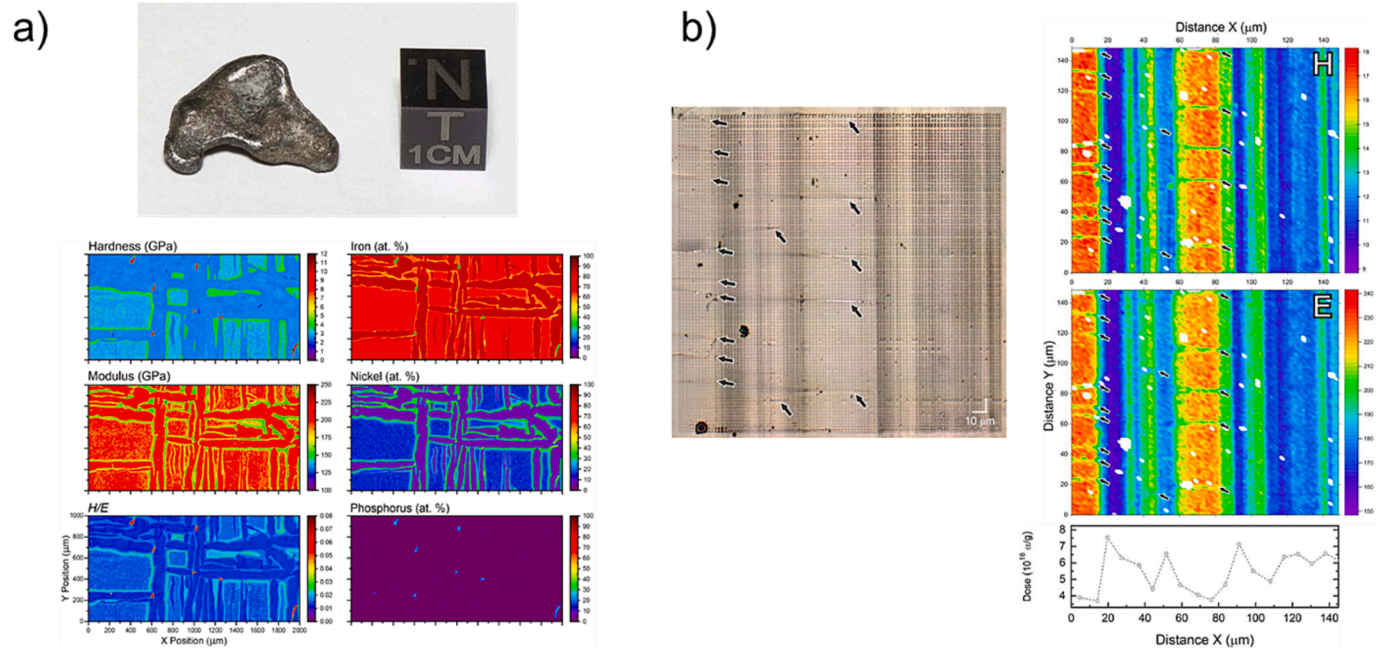

Fig. 21. High-speed nanoindentation in minerals. a) Taza meteorite microstructural mapping for Kamacite bands identification (reprinted and adapted from Wheeler, J. M. [45], Copyright(2021), with permission from Springer Nature) and b) high-speed mapping of radiation damaged Zircon (reproduced from Beirau, T. et al. [94]).

addition, the surrounding mineral matter led to confinement effects and enhanced elastic modulus values, while cracks and pores lowered the stiffness. The results suggest a declining trend with increasing maturity for elastic modulus, with no apparent relationship with thermal maturity for hardness. The study demonstrates a multimethod approach for fast and reliable assessment of representative material parameters from organic rock constituents.

6. Realtime high-temperature scanning indentation

From Section 2 of this review article, the reader should have acknowledged the methodological background behind high-speed nanoindentation mapping. Specifically, while the basic operational mode provides spatial information about the elastic modulus and hardness distribution at a certain target load or penetration depth, most of the recent year advancement brought nanoindenter manufacturers into allowing for the high-frequency acquisition of properties during the fast loading toward the target, thus enabling the so-called 4D mapping.

Therefore, HSNM can potentially be expanded for mapping additional properties to hardness and modulus, which require ad-hoc loading history and continuous extrapolation of the material's data during loading. As an example, when combined with HSNM, advanced spherical nanoindentation techniques may allow the characterization of spatial variations in yield strength and strain-hardening behavior.

Moreover, recent studies have shown that high-frequency data acquisition in nanoindentation allows for the extraction of strain rate sensitivity [35] and adhesion surface properties (surface free energy, [96]) on highly heterogeneous materials.

In this section, the authors would like to give a further outlook on HSNM future perspectives, focusing on specific loading histories developed for high-temperature investigation of materials properties through nanoindentation, on what could be considered a natural outgrowth of fast nanoindentation at high-frequency acquisition: realtime high-temperature scanning indentation. Indeed, traditional testing methods often involve slow indentation processes, limiting the ability to capture phenomena related to rapid changes in material response at different temperatures. However, with fast nanoindentation protocols (at the basis of HSNM), it becomes possible (i) to rapidly measure and evaluate the mechanical properties of temperature-dependent materials under various thermal conditions to (ii), in principle, perform isothermal measurement even while temperature gradients are present whenever the characteristic time constant of the temperature change is sensibly higher than the loading one. By applying controlled and rapid indentation cycles, these protocols allow for characterizing dynamic material behavior, such as viscoelasticity, creep, and stress relaxation, at elevated or reduced temperatures.

A recent study shows how high-speed nanoindentation can be used to investigate metallurgical evolution occurring during isothermal heat treatments [97], to measure elastic, plastic, and creep properties in metals. The method utilizes high-speed nanohardness measurements while linearly ramping the system's temperature with appropriate settings. The loading procedure consists of a quarter sinus loading function, a creep segment, and a three-step unloading method, allowing for the measurement of elastic, plastic, and creep properties (as shown in Fig. 22 on the left). **High-speed nanoindentation is crucial because isothermal testing is only achieved when the indentation cycle is limited to one second**. This methodology will allow further insights into the fundamental mechanisms underlying thermally activated physical transformations in heterogeneous metals, and has been successfully benchmarked on a binary model ZrCu TFMG to identify the physical transformations of the amorphous coatings, including the metallic glass-to-supercooled liquid transition and crystallization process [98] (Fig. 22). Expansion of HSNM into *operando* testing conditions may allow the assessment of the mechanical properties of entire microstructural cross-sections to be determined as a function of environmental conditions: high and low temperatures, humidity, radiation, and/or corrosion.

Along this line, this method's future directions come with novel material discoveries. They are expected to have a remarkable impact in critical research sectors, including relevant applications in additively manufactured complex materials for healthcare, transportation, and new energy markets. The ability of spatially resolved high-resolution property mapping as a function of time or temperature will open novel pathways for designing and developing new complex materials with improved performance and extended functional longevity.

7. Conclusions and future perspectives

High-speed nanoindentation mapping is a powerful technique for the mechanical characterization of materials microstructures and properties with high lateral resolution comparable to many microscopy techniques. In this article, we have reported relevant examples of the recent developments and applications of high-speed nanoindentation. Starting from the original idea of fast modulus and hardness mapping in

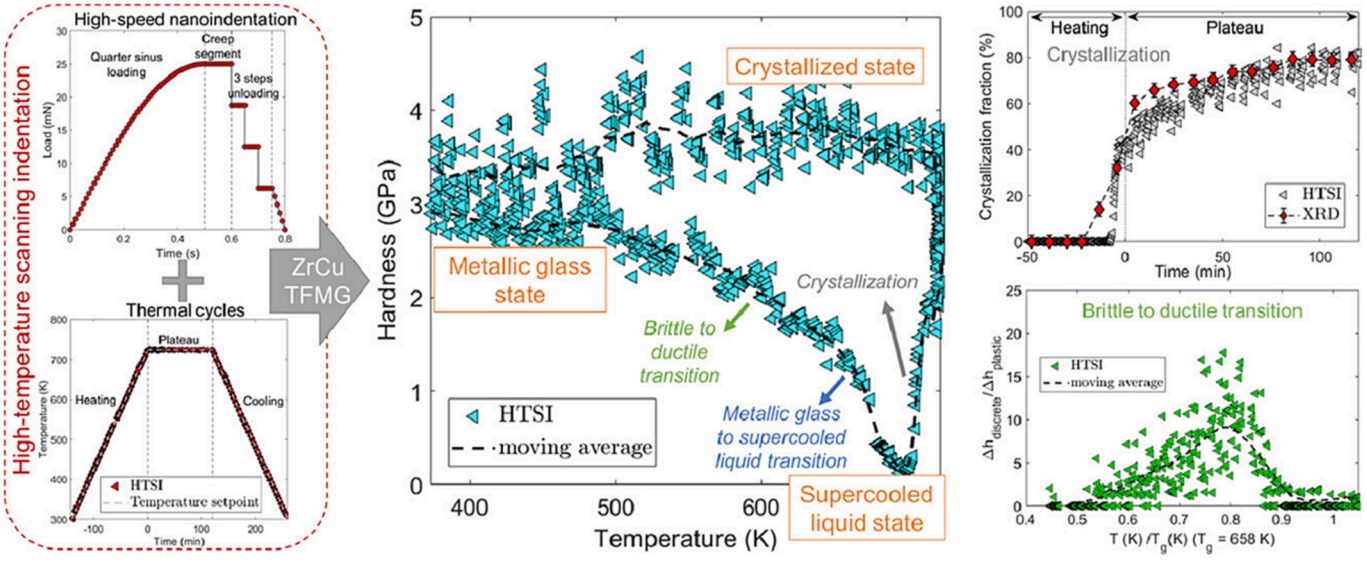

Fig. 22. a) Realtime high-temperature scanning indentation method overview and application for an-isothermal heat treatments in metallic glass films (reprinted from Comby-Dassonneville, S. et al. [98], Copyright(2021), with permission from Elsevier).

heterogeneous materials for statistical screening, this method has rapidly been established as a potent tool for high-throughput material screening. It can be an enabling technology for developing novel material formulations.

There are several technical issues that must be considered in the acquisition of high-speed nanoindentation maps. Indentations need to be appropriately spaced (10 d/h) for their maximum indentation depth to prevent interactions between neighboring indentations. This is easily achieved in displacement-controlled mapping, but this requires careful selection of the applied load in load-controlled maps. The lateral resolution of the maps is limited by the sharpness of the indenter probe to be ~150 nm, but this may be surpassed with sharper probes in softer materials. Conventional mechanical wear of the indenter has been observed not to be significant for current typical map sizes, but additional chemical effects at high temperatures are anticipated to be challenging. Current indentation mapping speeds yield an increase in indentation strain rate of ~2 orders of magnitude, which can produce increased measured hardness values in strain rate-sensitive materials. As test speeds increase, this may become a significant consideration.

The analysis of the literature has also shown that the further optimization of high-speed nanoindentation goes in parallel (and in full synergy) with the development of high-strain-rate nanoindentation testing and the recent advances in the use of artificial intelligence to the analysis of large nanoindentation datasets. These large datasets require new interpretation tools, such as statistically-aided techniques and artificial intelligence algorithms, to segment and process the data. In particular, the key aspect of future innovation will be given by combining innovative nanoindentation hardware with advanced data analysis and advanced microscopy tools, with a vision of developing high-performance data-augmented correlative mechanical microscopy tools.

The development of correlative mechanical microscopy techniques combining high-speed nanoindentation mapping with analytical electron microscopy techniques is already well underway. This is commonly done with visual correlations between maps acquired by different techniques without fully paired datasets. However, several authors have also successfully demonstrated fully registered datasets that correlate nanoindentation maps with EBSD and EDX to allow high-throughput determination of mechanical properties with crystal structure/orientation or composition. This greatly aids analysis methods for segmenting data by phase, orientation, or composition, and enables combinatorial studies with composition or statistical study of the influence of grain boundaries.

As with conventional nanoindentation, the success of high-speed nanoindentation mapping as a characterization technique is shown by its relatively rapid adoption and application to a wide range of different materials classes: complex metal alloys, sprayed coatings, composite materials, and natural materials. Nanoindentation mapping is expected to have applications in nearly all materials classes to which conventional nanoindentation has been applied and enable many new studies in these materials.

Declaration of Competing Interest

Jeffrey M. Wheeler is also employed by FemtoTools AG but received no financial support for this work. The remaining authors have no known competing financial interests or personal relationships that could have appeared to influence the work reported in this paper.

Data availability

Data will be made available on request.

Acknowledgments

E. Rossi and M. Sebastiani gratefully acknowledge partial financial support from the European Commission, European project NanoMECommons, grant agreement no. 952869.

References

[1] W.C. Oliver, G.M. Pharr, Measurement of hardness and elastic modulus by instrumented indentation: advances in understanding and refinements to methodology, J. Mater. Res. 19 (1) (2004) 3–20, https://doi.org/10.1557/jmr.2004.19.1.3.
[2] W.C. Oliver, G.M. Pharr, An improved technique for determining hardness and elastic modulus using load and displacement sensing indentation experiments, J. Mater. Res. 7 (6) (1992) 1564–1583, https://doi.org/10.1557/jmr.1992.1564.
[3] J.B. Pethicai, R. Hutchings, W.C. Oliver, Hardness measurement at penetration depths as small as 20 nm, Philos. Mag. A: Phys. Condens. Matter, Struct., Defects Mech. Properties 48 (4) (1983) 593–606, https://doi.org/10.1080/01418618308234914.
[4] S.J. Marshall, M. Balooch, S. Habelitz, G. Balooch, R. Gallagher, G.W. Marshall, The dentin - enamel junction - a natural, multilevel interface, J. Eur. Ceram. Soc. 23 (15) (2003) 2897–2904, https://doi.org/10.1016/S0955-2219(03)00301-7.
[5] G. Balooch, G.W. Marshall, S.J. Marshall, O.L. Warren, S.A.S. Asif, M. Balooch, Evaluation of a new modulus mapping technique to investigate microstructural features of human teeth, J. Biomech. 37 (8) (2004) 1223–1232, https://doi.org/10.1016/j.jbiomech.2003.12.012.
[6] G. Constantinides, F.J. Ulm, The effect of two types of C-S-H on the elasticity of cement-based materials: Results from nanoindentation and micromechanical modeling, Cem. Concr. Res. 34 (1) (Jan. 2004) 67–80, https://doi.org/10.1016/S0008-8846(03)00230-8.
[7] G. Constantinides, K.S. Ravi Chandran, F.J. Ulm, K.J. Van Vliet, Grid indentation analysis of composite microstructure and mechanics: principles and validation, Mater. Sci. Eng. A 430 (1–2) (2006) 189–202, https://doi.org/10.1016/j.msea.2006.05.125.
[8] G. Constantinides, F.J. Ulm, The nanogranular nature of C-S-H, J. Mech. Phys. Solids 55 (1) (Jan. 2007) 64–90, https://doi.org/10.1016/j.jmps.2006.06.003.
[9] N.X. Randall, M. Vandamme, F.J. Ulm, Nanoindentation analysis as a two-dimensional tool for mapping the mechanical properties of complex surfaces, J. Mater. Res. 24 (3) (2009) 679–690, https://doi.org/10.1557/jmr.2009.0149.
[10] M. Vandamme, F.J. Ulm, P. Fonollosa, Nanogranular packing of C-S-H at substochiometric conditions, Cem. Concr. Res. 40 (1) (Jan. 2010) 14–26, https://doi.org/10.1016/j.cemconres.2009.09.017.
[11] M. Miller, C. Bobko, M. Vandamme, F.J. Ulm, Surface roughness criteria for cement paste nanoindentation, Cem. Concr. Res. 38 (4) (2008) 467–476, https://doi.org/10.1016/j.cemconres.2007.11.014.
[12] P. Sudharshan Phani, W. C. Oliver, A critical assessment of the effect of indentation spacing on the measurement of hardness and modulus using instrumented indentation testing Mater. Des., 164 (Feb. 2019) 107563, 10.1016/j.matdes.2018.107563.
[13] M. Sebastiani, R. Moscatelli, F. Ridi, P. Baglioni, F. Carassiti, High-resolution high-speed nanoindentation mapping of cement pastes: Unravelling the effect of microstructure on the mechanical properties of hydrated phases, Mater. Des. 97 (May 2016) 372–380, https://doi.org/10.1016/j.matdes.2016.02.087.
[14] M.Z. Mughal, H.-Y. Amanieu, R. Moscatelli, M. Sebastiani, A comparison of microscale techniques for determining fracture toughness of LiMn<inf>2</inf>O<inf>4</inf> particles, Materials 10 (4) (2017) 403, https://doi.org/10.3390/ma10040403.
[15] H.Y. Amanieu, D. Rosato, M. Sebastiani, F. Massimi, D.C. Lupascu, Mechanical property measurements of heterogeneous materials by selective nanoindentation: application to LiMn2O4 cathode, Mater. Sci. Eng. A 593 (Jan. 2014) 92–102, https://doi.org/10.1016/j.msea.2013.11.044.
[16] M.Z. Mughal, R. Moscatelli, H.Y. Amanieu, M. Sebastiani, Effect of lithiation on micro-scale fracture toughness of LixMn2O4 cathode, Scr. Mater. 116 (2016) 62–66, https://doi.org/10.1016/j.scriptamat.2016.01.023.
[17] J.L. Hay, P. Agee, Mapping the mechanical properties of alloyed magnesium (AZ 61), Mag. Technol. (2013) 329–332, https://doi.org/10.1002/9781118663004.ch55.
[18] J.M. Wheeler, B. Gan, R. Spolenak, Combinatorial investigation of the Ni–Ta system via correlated high-speed nanoindentation and EDX mapping, Small Methods 6 (2) (2022), https://doi.org/10.1002/smtd.202101084.
[19] J. Konnerth, A. Valla, W. Gindl, Nanoindentation mapping of a wood-adhesive bond, Appl. Phys. A Mater. Sci. Process. 88 (2) (2007) 371–375, https://doi.org/10.1007/s00339-007-3976-y.
[20] L.S. de Vasconcelos, R. Xu, J. Li, K. Zhao, Grid indentation analysis of mechanical properties of composite electrodes in Li-ion batteries, Extreme Mech. Lett. 9 (Dec. 2016) 495–502, https://doi.org/10.1016/j.eml.2016.03.002.
[21] F.J. Ulm, et al., Does microstructure matter for statistical nanoindentation techniques? Cem. Concr. Compos. 32 (1) (Jan. 2010) 92–99, https://doi.org/10.1016/j.cemconcomp.2009.08.007.
[22] L.E. Samuels, T.O. Mulhearn, An experimental investigation of the deformed zone associated with indentation hardness impressions, J. Mech. Phys. Solids 5 (2) (Mar. 1957) 125–134, https://doi.org/10.1016/0022-5096(57)90056-X.
[23] H. Besharatloo, J.M. Wheeler, Influence of indentation size and spacing on statistical phase analysis via high-speed nanoindentation mapping of metal alloys, J. Mater. Res. 36 (11) (2021) 2198–2212, https://doi.org/10.1557/s43578-021-00214-5.
[24] G.M. Pharr, E.G. Herbert, Y. Gao, The indentation size effect: a critical examination of experimental observations and mechanistic interpretations, https://doi.org/

10.1146/annurev-matsci-070909-104456 40 (Jul. 2010) 271–292, 10.1146/ANNUREV-MATSCI-070909-104456.
[25] S. Pathak, D. Stojakovic, R. Doherty, S.R. Kalidindi, Importance of surface preparation on the nano-indentation stress-strain curves measured in metals, J. Mater. Res. 24 (3) (Mar. 2009) 1142–1155, https://doi.org/10.1557/JMR.2009.0137/METRICS.
[26] E.D. Hintsala, U. Hangen, D.D. Stauffer, High-throughput nanoindentation for statistical and spatial property determination, JOM 70 (4) (Apr. 2018) 494–503, https://doi.org/10.1007/s11837-018-2752-0.
[27] J. Nohava, J. Čech, M. Havlíček, R. Consiglio, Indenter wear study and proposal of a simple method for evaluation of indenter blunting, J. Mater. Res. 36 (21) (Nov. 2021) 4449–4459, https://doi.org/10.1557/s43578-021-00401-4.
[28] K.D. Bouzakis, M. Pappa, G. Maliaris, N. Michailidis, Fast determination of parameters describing manufacturing imperfections and operation wear of nanoindenter tips, Surf. Coat. Technol. 215 (Jan. 2013) 218–223, https://doi.org/10.1016/J.SURFCOAT.2012.09.061.
[29] J.M. Wheeler, D.E.J. Armstrong, W. Heinz, R. Schwaiger, High temperature nanoindentation: the state of the art and future challenges, Curr. Opin. Solid State Mater. Sci. 19 (6) (Dec. 2015) 354–366, https://doi.org/10.1016/J.COSSMS.2015.02.002.
[30] J.M. Wheeler, J. Michler, Invited article: Indenter materials for high temperature nanoindentation, Rev. Sci. Instrum. 84 (10) (Oct. 2013), 101301, https://doi.org/10.1063/1.4824710/360481.
[31] M.A. Monclús, S. Lotfian, J.M. Molina-Aldareguía, Tip shape effect on hot nanoindentation hardness and modulus measurements, Int. J. Precis. Eng. Manuf. 15 (8) (Aug. 2014) 1513–1519, https://doi.org/10.1007/S12541-014-0499-2/METRICS.
[32] C. Minnert, W.C. Oliver, K. Durst, New ultra-high temperature nanoindentation system for operating at up to 1100 °C, Mater. Des. 192 (Jul. 2020), 108727, https://doi.org/10.1016/J.MATDES.2020.108727.
[33] B. Merle, W.H. Higgins, G.M. Pharr, Critical issues in conducting constant strain rate nanoindentation tests at higher strain rates, J. Mater. Res. 34 (20) (Oct. 2019) 3495–3503, https://doi.org/10.1557/JMR.2019.292.
[34] B.N. Lucas, W.C. Oliver, Indentation power-law creep of high-purity indium, Metall. Mater. Trans. A 30 (3) (Mar. 1999) 601–610, https://doi.org/10.1007/S11661-999-0051-7/METRICS.
[35] P.S. Phani, W.C. Oliver, Ultra high strain rate nanoindentation testing, Materials 10 (6) (Jun. 2017) 663, https://doi.org/10.3390/ma10060663.
[36] V. Maier, K. Durst, J. Mueller, B. Backes, H.W. Höppel, M. Göken, Nanoindentation strain-rate jump tests for determining the local strain-rate sensitivity in nanocrystalline Ni and ultrafine-grained Al, J. Mater. Res. 26 (11) (Jun. 2011) 1421–1430, https://doi.org/10.1557/JMR.2011.156.
[37] ISO/TC 164/SC 3 Hardness testing, Metallic materials — Instrumented indentation test for hardness and materials parameters — Part 1: Test method. 2015, p. 46. https://www.iso.org/standard/56626.html.
[38] A.L.M. Vargas, E. Blando, R. Hübler, Elasto – Plastic materials behavior evaluation according to different models applied in indentation hardness tests, Measurement 139 (Jun. 2019) 134–139, https://doi.org/10.1016/J.MEASUREMENT.2019.01.090.
[39] M. Braunovic, L. Rodrigue, D. Gagnon, Nanoindentation study of intermetallic phases in Al-Cu bimetallic system, in: Electrical Contacts, Proceedings of the Annual Holm Conference on Electrical Contacts, 2008, pp. 270–275, https://doi.org/10.1109/HOLM.2008.ECP.55.
[40] K.S. Lee, Y.N. Kwon, Solid-state bonding between Al and Cu by vacuum hot pressing, Trans. Nonferrous Met. Soc. Chin. 23 (2) (Feb. 2013) 341–346, https://doi.org/10.1016/S1003-6326(13)62467-X.
[41] B. Merle, V. Maier-Kiener, G.M. Pharr, Influence of modulus-to-hardness ratio and harmonic parameters on continuous stiffness measurement during nanoindentation, Acta Mater. 134 (Aug. 2017) 167–176, https://doi.org/10.1016/j.actamat.2017.05.036.
[42] P.S. Phani, W.C. Oliver, G.M. Pharr, Understanding and modeling plasticity error during nanoindentation with continuous stiffness measurement, Mater. Des. 194 (Sep. 2020), 108923, https://doi.org/10.1016/j.matdes.2020.108923.
[43] F.J. Ulm, M. Vandamme, C. Bobko, J. Alberto Ortega, K. Tai, C. Ortiz, Statistical indentation techniques for hydrated nanocomposites: Concrete, bone, and shale, J. Am. Ceram. Soc. 90 (9) (2007) 2677–2692, https://doi.org/10.1111/j.1551-2916.2007.02012.x.
[44] Z. Zhang, J. Qin, Z. Ma, X. Pang, Y. Zhou, Comparison of three different deconvolution methods for analyzing nanoindentation test data of hydrated cement paste, Cem. Concr. Compos. 138 (Apr. 2023), 104990, https://doi.org/10.1016/J.CEMCONCOMP.2023.104990.
[45] J.M. Wheeler, Mechanical phase mapping of the Taza meteorite using correlated high-speed nanoindentation and EDX, J. Mater. Res. 36 (1) (Jan. 2021) 94–104, https://doi.org/10.1557/s43578-020-00056-7.
[46] H. Besharatloo, et al., Novel mechanical characterization of austenite and ferrite phases within duplex stainless steel, Metals (Basel) 10 (10) (Oct. 2020) 1–15, https://doi.org/10.3390/met10101352.
[47] Y. Xiao, H. Besharatloo, B. Gan, X. Maeder, R. Spolenak, J.M. Wheeler, Combinatorial investigation of Al–Cu intermetallics using small-scale mechanical testing, J. Alloy. Compd. 822 (May 2020), 153536, https://doi.org/10.1016/J.JALLCOM.2019.153536.
[48] J.J. Roa, P. Sudharshan Phani, W.C. Oliver, L. Llanes, Mapping of mechanical properties at microstructural length scale in WC-Co cemented carbides: assessment of hardness and elastic modulus by means of high speed massive nanoindentation and statistical analysis, Int. J. Refract Metals Hard Mater. 75 (Sep. 2018) 211–217, https://doi.org/10.1016/j.ijrmhm.2018.04.019.
[49] B. Vignesh, W.C. Oliver, G.S. Kumar, P.S. Phani, Critical assessment of high speed nanoindentation mapping technique and data deconvolution on thermal barrier coatings, Mater. Des. 181 (Nov. 2019), 108084, https://doi.org/10.1016/j.matdes.2019.108084.
[50] E.P. Koumoulos, K. Paraskevoudis, C.A. Charitidis, Constituents phase reconstruction through applied machine learning in nanoindentation mapping data of mortar surface, J. Compos. Sci. 3 (3) (2019) 63, https://doi.org/10.3390/jcs3030063.
[51] B.C. Sousa, C. Viera, R. Neamtu, D.L. Cote, Clustering algorithms for nanomechanical property mapping and resultant microstructural constituent and phase quantification, Min. Met. Mater. Ser. (2022) 713–724, https://doi.org/10.1007/978-3-030-92381-5_68/COVER.
[52] S. Vranjes-Wessely, et al., High-speed nanoindentation mapping of organic matter-rich rocks: a critical evaluation by correlative imaging and machine learning data analysis, Int. J. Coal Geol. 247 (Nov. 2021), 103847, https://doi.org/10.1016/j.coal.2021.103847.
[53] G. Konstantopoulos, E.P. Koumoulos, C.A. Charitidis, Classification of mechanism of reinforcement in the fiber-matrix interface: application of Machine Learning on nanoindentation data, Mater. Des. 192 (2020), 108705, https://doi.org/10.1016/j.matdes.2020.108705.
[54] S. Kossman, M. Bigerelle, Pop-in identification in nanoindentation curves with deep learning algorithms, Materials 14 (22) (2021), https://doi.org/10.3390/ma14227027.
[55] G. Bianco, T. Paul, A. Nisar, A. Hamrani, B. Boesl, A. Agarwal, Nanoindentation mapping defects filtration for heterogeneous materials using generative adversarial networks, Mater. Charact. 191 (May) (2022), 112107, https://doi.org/10.1016/j.matchar.2022.112107.
[56] D.L. Joslin, W.C. Oliver, A new method for analyzing data from continuous depth-sensing microindentation tests, J. Mater. Res. 5 (1) (Jan. 1990) 123–126, https://doi.org/10.1557/JMR.1990.0123.
[57] D. Gu, X. Shi, R. Poprawe, D. L. Bourell, R. Setchi, J. Zhu, Material-structure-performance integrated laser-metal additive manufacturing, Science (1979) 372 (6545) (May 2021), 10.1126/SCIENCE.ABG1487/ASSET/C9C9DF6C-17D9-4FC4-9AD2-001ACE3899FC/ASSETS/GRAPHIC/372_ABG1487_F5.JPEG.
[58] T. Keil, E. Bruder, K. Durst, Exploring the compositional parameter space of high-entropy alloys using a diffusion couple approach, Mater. Des. 176 (Aug. 2019), 107816, https://doi.org/10.1016/J.MATDES.2019.107816.
[59] J.C. Zhao, A combinatorial approach for efficient mapping of phase diagrams and properties, J. Mater. Res. 16 (6) (Jun. 2001) 1565–1578, https://doi.org/10.1557/JMR.2001.0218/METRICS.
[60] C.M. Magazzeni, et al., Nanoindentation in multi-modal map combinations: a correlative approach to local mechanical property assessment, J. Mater. Res. 36 (11) (Jun. 2021) 2235–2250, https://doi.org/10.1557/s43578-020-00035-y.
[61] W. Wilson, L. Sorelli, A. Tagnit-Hamou, Automated coupling of NanoIndentation and Quantitative Energy-Dispersive Spectroscopy (NI-QEDS): a comprehensive method to disclose the micro-chemo-mechanical properties of cement pastes, Cem. Concr. Res. 103 (Jan. 2018) 49–65, https://doi.org/10.1016/j.cemconres.2017.08.016.
[62] Y. Kok, et al., Anisotropy and heterogeneity of microstructure and mechanical properties in metal additive manufacturing: A critical review, Mater. Des. 139 (Feb. 2018) 565–586, https://doi.org/10.1016/J.MATDES.2017.11.021.
[63] T. Fongsamootr, I. Thawon, N. Tippayawong, K.Y. Tippayawong, P. Suttakul, Effect of print parameters on additive manufacturing of metallic parts: performance and sustainability aspects, Sci. Rep. 12 (1) (Nov 2022) 1–12, https://doi.org/10.1038/s41598-022-22613-2.
[64] H.M. Gardner, et al., Quantifying the effect of oxygen on micro-mechanical properties of a near-alpha titanium alloy, J. Mater. Res. 36 (12) (Jun. 2021) 2529–2544, https://doi.org/10.1557/S43578-020-00006-3/FIGURES/9.
[65] Z. Liu, J. Zhang, B. He, Y. Zou, High-speed nanoindentation mapping of a near-alpha titanium alloy made by additive manufacturing, J. Mater. Res. 36 (11) (Jun. 2021) 2223–2234, https://doi.org/10.1557/S43578-021-00204-7/FIGURES/9.
[66] Z. Liu, R. Li, D. Chen, Y. Sun, B. He, Y. Zou, Enhanced tensile ductility of an additively manufactured near-α titanium alloy by microscale shear banding, Int. J. Plast 157 (Oct. 2022), 103387, https://doi.org/10.1016/J.IJPLAS.2022.103387.
[67] S. Shakerin, M. Sanjari, B.S. Amirkhiz, M. Mohammadi, Interface engineering of additively manufactured maraging steel-H13 bimetallic structures, Mater Charact 170 (June) (Dec. 2020), 110728, https://doi.org/10.1016/j.matchar.2020.110728.
[68] M.A. Wagner, et al., Filament extrusion-based additive manufacturing of 316L stainless steel: effects of sintering conditions on the microstructure and mechanical properties, Addit. Manuf. 59 (Nov. 2022), 103147, https://doi.org/10.1016/j.addma.2022.103147.
[69] D. Raabe, C.C. Tasan, H. Springer, M. Bausch, From high-entropy alloys to high-entropy steels, Steel Res. Int. 86 (10) (Oct. 2015) 1127–1138, https://doi.org/10.1002/SRIN.201500133.
[70] H.J. Qu, J.P. Wharry, Nanoindentation investigation of chloride-induced stress corrosion crack propagation in an austenitic stainless steel weld, Metals (Basel) 12 (8) (Aug. 2022) 1243, https://doi.org/10.3390/met12081243.
[71] S. Janakiram, P.S. Phani, G. Ummethala, S.K. Malladi, J. Gautam, L.A.I. Kestens, New insights on recovery and early recrystallization of ferrite-pearlite banded cold rolled high strength steels by high speed nanoindentation mapping, Scr. Mater. 194 (Mar. 2021), 113676, https://doi.org/10.1016/j.scriptamat.2020.113676.
[72] D. G. Kalali, H. Seekala, P. S. Phani, K. Bhanu Sankara Rao, K. V. Rajulapati, High speed nanoindentation aided correlative study between local mechanical properties and chemical segregation in equiatomic MoNb and MoNbTi alloys, J. Mater. Res. (2023), 10.1557/S43578-023-01007-8.

[73] A. Meghwal et al., Structure-property correlation of a CoCrFeNi medium-entropy alloy manufactured using extreme high-speed laser material deposition (EHLA), Intermetallics (Barking), 152 (Jan. 2023) 107769, 10.1016/J.INTERMET.2022.107769.
[74] A. Dhal, R. Sankar Haridas, P. Agrawal, S. Gupta, R.S. Mishra, Mapping hierarchical and heterogeneous micromechanics of a transformative high entropy alloy by nanoindentation and machine learning augmented clustering, Mater. Des. 230 (Jun. 2023), 111957, https://doi.org/10.1016/J.MATDES.2023.111957.
[75] J. Němeček, J. Němeček, J. Lukeš, High-speed mechanical mapping of blended cement pastes and its comparison with standard modes of nanoindentation, Mater. Today Commun. 23 (Jun. 2020), 100806, https://doi.org/10.1016/j.mtcomm.2019.100806.
[76] H. Besharatloo, et al., Carbon addition effects on microstructure and small-scale hardness for Ti(C, N)-FeNi cermets, Int. J. Refract. Metals Hard Mater. 85 (Dec. 2019), 105064, https://doi.org/10.1016/j.ijrmhm.2019.105064.
[77] S. Mubina, P. Sudharshan Phani, A.K. Khanra, B.P. Saha, A nanoindentation based study to evaluate the effect of carbon nanofibers on the mechanical properties of SiC composites, Compos. Interfaces 28 (4) (2021) 363–380, https://doi.org/10.1080/09276440.2020.1780555.
[78] S. Gordon, et al., Micromechanical mapping of polycrystalline cubic boron nitride composites by means of high-speed nanoindentation: assessment of microstructural assemblage effects, J. Eur. Ceram. Soc. 43 (7) (Jul. 2023) 2968–2975, https://doi.org/10.1016/j.jeurceramsoc.2022.08.047.
[79] M. Lilli, et al., Quantitative multi-scale characterization of single basalt fibres: Insights into strength loss mechanisms after thermal conditioning, Mater. Sci. Eng. A 797 (Oct. 2020), 139963, https://doi.org/10.1016/j.msea.2020.139963.
[80] A.B. Irez, J. Hay, I. Miskioglu, E. Bayraktar, Scrap-rubber based composites reinforced with boron and alumina, Conf. Proc. Soc. Exp. Mech. Ser. 6 (2018) 1–9, https://doi.org/10.1007/978-3-319-63408-1_1.
[81] R. Daniel, J. Musil, Novel Nanocomposite Coatings: Advances and Industrial Applications, CRC Press, 2013.
[82] P. Suresh Babu, P. Chanikya Rao, A. Jyothirmayi, P. Sudharshan Phani, L. Rama Krishna, D. Srinivasa Rao, Evaluation of microstructure, property and performance of detonation sprayed WC-(W, Cr)2C-Ni coatings, Surf. Coat. Technol. 335 (2018) 345–354, https://doi.org/10.1016/j.surfcoat.2017.12.055.
[83] A. Rico, J. Gómez-García, C.J. Múnez, P. Poza, V. Utrilla, Mechanical properties of thermal barrier coatings after isothermal oxidation. Depth sensing indentation analysis, Surf. Coat. Technol. 203 (16) (May 2009) 2307–2314, https://doi.org/10.1016/j.surfcoat.2009.02.035.
[84] J.A. Thompson, T.W. Clyne, The effect of heat treatment on the stiffness of zirconia top coats in plasma-sprayed TBCs, Acta Mater. 49 (9) (May 2001) 1565–1575, https://doi.org/10.1016/S1359-6454(01)00065-9.
[85] Q. Chen, W.G. Mao, Y.C. Zhou, C. Lu, Effect of Young's modulus evolution on residual stress measurement of thermal barrier coatings by X-ray diffraction, Appl. Surf. Sci. 256 (23) (Sep. 2010) 7311–7315, https://doi.org/10.1016/j.apsusc.2010.05.071.
[86] G. Bolelli, M.G. Righi, M.Z. Mughal, R. Moscatelli, O. Ligabue, N. Antolotti, M. Sebastiani, L. Lusvarghi, E. Bemporad, Damage progression in thermal barrier coating systems during thermal cycling: A nano-mechanical assessment, Materials and Design 166 (2019) 107615, https://doi.org/10.1016/j.matdes.2019.107615.
[87] M.F. Doerner, W.D. Nix, A method for interpreting the data from depth-sensing indentation instruments, J. Mater. Res. 1 (4) (1986) 601–609, https://doi.org/10.1557/JMR.1986.0601.
[88] T.Y. Tsui, G.M. Pharr, Substrate effects on nanoindentation mechanical property measurement of soft films on hard substrates, J. Mater. Res. 14 (1) (Jul. 1999) 292–301, https://doi.org/10.1557/JMR.1999.0042/METRICS.
[89] R. Saha, W.D. Nix, Effects of the substrate on the determination of thin film mechanical properties by nanoindentation, Acta Mater. 50 (1) (Jan. 2002) 23–38, https://doi.org/10.1016/S1359-6454(01)00328-7.
[90] J. Hay, B. Crawford, Measuring substrate-independent modulus of thin films, J. Mater. Res. 26 (6) (Mar. 2011) 727–738, https://doi.org/10.1557/JMR.2011.8.
[91] L. Qin, L. Lin, F. Fu, M. Fan, Micromechanical properties of wood cell wall and interface compound middle lamella using quasi-static nanoindentation and dynamic modulus mapping, J. Mater. Sci. 53 (1) (Jan. 2018) 549–558, https://doi.org/10.1007/s10853-017-1185-4.
[92] P. Klímek, V. Sebera, D. Tytko, M. Brabec, J. Lukeš, Micromechanical properties of beech cell wall measured by micropillar compression test and nanoindentation mapping, Holzforschung 74 (9) (2020) 899–904, https://doi.org/10.1515/hf-2019-0128.
[93] C. Xu, et al., Large-scale and high-resolution visualization of static mechanical properties of wood-adhesive interphase utilizing nanoindentation mapping, Wood Sci. Technol. 56 (4) (Jul. 2022) 1029–1045, https://doi.org/10.1007/s00226-022-01394-x.
[94] T. Beirau, W.C. Oliver, C.E. Reissner, W.D. Nix, H. Pöllmann, R.C. Ewing, Radiation-damage in multi-layered zircon: mechanical properties, Appl. Phys. Lett. 115 (8) (Aug. 2019) 81902, https://doi.org/10.1063/1.5119207/38573.
[95] T. Beirau, E. Rossi, M. Sebastiani, W.C. Oliver, H. Pöllmann, R.C. Ewing, Fracture toughness of radiation-damaged zircon studied by nanoindentation pillar-splitting, Appl. Phys. Lett. 119 (23) (Dec. 2021), 231903, https://doi.org/10.1063/5.0070597.
[96] E.M. Rossi, et al., A novel nanoindentation protocol to characterize surface free energy of superhydrophobic nanopatterned materials, J. Mater. Res. 36 (11) (Jun. 2021) 2357–2370, https://doi.org/10.1557/s43578-021-00127-3.
[97] G. Tiphéne, et al., High-temperature scanning indentation: A new method to investigate in situ metallurgical evolution along temperature ramps, J. Mater. Res. 36 (12) (Jun. 2021) 2383–2396, https://doi.org/10.1557/s43578-021-00107-7.
[98] S. Comby-Dassonneville, et al., Real-time high-temperature scanning indentation: probing physical changes in thin-film metallic glasses, Appl. Mater. Today 24 (2021), https://doi.org/10.1016/j.apmt.2021.101126.